Targeted Mutation Detection in Advanced Breast Cancer Using MammaSeq™ Identifies RET as a Potential Contributor to Breast Cancer Metastasis

By

Nicholas George Smith

B.S., Biomolecular Science, Clarkson University, 2014

Submitted to the Graduate Faculty of

the School of Medicine in partial fulfillment

of the requirements for the degree of

MS in Molecular Pharmacology

University of Pittsburgh

2018

UNIVERSITY OF PITTSBURGH

SCHOOL OF MEDICINE

This dissertation was presented

By

Nicholas George Smith

It was defended on

June 27th, 2018

and approved by

Qiming Jane Wang, PhD, Associate Professor, Pharmacology & Chemical Biology

Adrian V. Lee, PhD, Professor, Pharmacology & Chemical Biology

Steffi Oesterreich, PhD, Professor, Pharmacology & Chemical Biology

Gary Kohanbash, PhD, Assistant Professor, Neurosurgery

Targeted Mutation Detection in Advanced Breast Cancer Using MammaSeq™ Identifies RET as a Potential Contributor to Breast Cancer Metastasis

Nicholas Smith

University of Pittsburgh, 2018

The lack of any reported breast cancer specific diagnostic NGS tests inspired the development of MammaSeq, an amplicon based NGS panel built specifically for use in advanced breast cancer. In a pilot study to define the clinical utility of the panel, 46 solid tumor samples, plus an additional 14 samples of circulating-free DNA (cfDNA) from patients with advanced breast cancer were sequenced and analyzed using the OncoKB precision oncology database. We identified 26 clinically actionable variants (levels 1-3) annotated by the OncoKB precision oncology database, distributed across 20 out of 46 solid tumor cases (40%), and 4 clinically actionable mutations distributed across 4 samples in the 14 cfDNA sample cohort (29%). The mutation allele (MAF) frequencies of ESR1-D538G and FOXA1-Y175C mutations correlated with CA.27.29 levels in patient-matched blood, indicating that MAF may be a reliable marker for disease burden. Interestingly, 4 of the mutations found in metastatic samples occurred in the gene RET, an oncogenic receptor tyrosine kinase. In an orthogonal study, the lab has recently identified RET as one of the most recurrently upregulated genes in breast cancer brain metastases. Interestingly, the ligand for RET is the family of glial-cell derived neurotrophic factors (GDNF), a growth factor secreted by glial cells of the central nervous system. This lead to the hypothesis that RET overexpression facilitates breast cancer brain metastasis in response to the high levels of GDNF, while RET activating point mutations increase metastatic capacity without specific organ tropism. While the effect of GDNF treatment on proliferation in 2D was limited, in ultra-low attachment

(ULA) plates we saw a significant increase in anchorage independent growth of MCF-7 cells. To determine if GDNF acts as a chemoattractant for RET positive BrCa cells, we utilized a transwell migration assay, with GDNF as the sole chemoattractant. When RET was overexpressed, there was a visual increase in cell migration. Together, these studies demonstrate the clinical feasibility of using MammaSeq to detect clinically actionable mutations in breast cancer patients, and provides provisional data supporting the investigation of RET signaling as a potentially targetable mediator of breast cancer brain metastasis.

Table of Contents

List of Abbreviations

BrCa	Breast Cancer
CCLE	Cancer Cell Line Encyclopedia
cfDNA	Circulating Cell-Free DNA
ER	Estrogen Receptor
GFAP	Glial Fibrillary Acidic Protein
GFR	Growth Factor Receptor
HR	Hormone Receptor
IDC	Invasive Ductal Carcinoma
ILC	Invasive Lobular Carcinoma
METABRIC	Molecular Taxonomy of Breast Cancer International Consrotium
NGS	Next-Generation Sequencing
RTK	Receptor Tyrosine Kinase
TCGA	The Cancer Genome Atlas
TPM	Transcripts per Million Reads
ULA	Ultra Low Attachment Plate
PR	Progesterone Receptor
SERM	Slelective Estrogen Receptor Modulator
SERD	Selective Estrogen Receptor Degrader
ddPCR	Droplet-Digital PCR
MBC	Metastatic Breast Cancer
GO	Gene Ontology
FDA	Food and Drug Administration
SMG	Significantly Mutated Genes
ISP	Ion Sphere Particle
CNV	Copy Number Variant
SNP	Single Nucleotide Polymorphism
gDNA	Germline DNA
IQR	Inter-quartile Range
SNV	Single Nucleotide Variant
MEN2	Multiple Endocrine Neoplasia Type-2
WES	Whole Exome Sequencing
TMB	Tumor Mutation Burden
IHC	Immunohistochemistry

List of Tables

List of Figures

1.0 INTRODUCTION

Breast cancer (BrCa) is the second leading cause of cancer death among women, accounting for more than 40,000 deaths each year in the United States alone[1]. While incidence has increased over the past 5 years, outcomes have consistently improved, with a current 5-year survival rate over 90%[2]. This improvement is largely due to advances in detection methods and the success of targeted therapies, driven by breakthroughs in understanding the molecular mechanisms of the disease.

1.1 Breast Cancer and Precision Medicine

BrCa has served as the model success story for precision medicine as targeted therapies represent front line therapy for roughly 85% of BrCa patients, either through endocrine therapies or HER2 targeting therapies. The most primitive form of endocrine therapy started in 1895 when George Thomas Beatson performed a bilateral oophorectomy on a patient with recurrent breast cancer, leading to complete remission and 4 years of post-surgery survival[3]. In 1872, Alfred Heger, who was treating a benign disease at the time, noted the physiological effects of an oophorectomy, the first documented case of surgical menopause. 10 years later, Thomas William Nunn reported a case of a women with breast cancer, who's disease completely regressed 6 months after her menstruation ceased[4]. Although these 3 investigators did not know it at the time, they demonstrated the relationship between the ovaries, estrogen, and mammary cancers.

Nearly 100 years later, in 1971 Jensen *et al*. noted the association between estrogen receptor (ER - Primarily ERα encoded by the gene *ESR1*) expression and patient response to adrenalectomies [5](in pre-menopausal women the vast majority of estrogen is produced in the ovaries, in post-menopausal women limited amounts of estrogen are produced in a variety of secondary organs including the adrenal glands). This led to the notion of estrogen and the ER as

being drivers in the vast majority of breast cancers. In 1977, tamoxifen, an ER antagonist that was originally developed as a contraceptive, gained FDA approval for the treatment of advanced BrCa. This was the first form of a targeted therapy for the treatment of cancer[6].

HER2, the other major biomarker that guides treatment decisions in BrCa, is a more straight-forward success story. The gene (*ERBB2*) was found to be amplified in a BrCa cell line, inspiring Dennis Salmon *et al*. to screen a large cohort of breast tumor samples. They found that gene was amplified is nearly 30% breast cancers [7] (more recent studies estimate it is actually closer to 20%[8]). This lead to the development of trastuzumab, a humanized monoclonal antibody targeting the extracellular domain of the receptor - approved for the treatment of HER2 positive BrCa in 1998[9]. This concept of developing targeted therapies specific for driver events, and tailoring treatment regimens for individual tumors is the backbone of precision medicine.

1.2 Subtypes of Breast Cancer

Despite falling under the umbrella of a single name, BrCa is not a single disease. Accumulating evidence suggests that subsets of BrCa with unique histopathological and molecular characteristics display different patterns of behavior and different responses to therapies[10]. Therefore, accurately stratifying patients into clinically relevant subgroups is of particular importance for therapeutic decision making.

From a histopathological perspective, there are two major subtypes of BrCa; invasive ductal carcinoma (IDC) and invasive lobular carcinoma (ILC). IDC accounts for roughly 80% of all diagnosed BrCa cases, while ILC accounts for 10-15% and several other rare subtypes account for the remaining 5-10%[11]. ILCs, typically diagnosed by a pathologist with classical H&E staining, have a unique linear, discohesive growth pattern, the result of the loss of functional E-

Cadherin. Previous studies have shown the E-Cadherin is lost at the protein level in 90-100% of ILC tumors[12].

Currently, therapeutic decisions are driven by classic immunohistochemistry (IHC) markers, including the estrogen receptor, progesterone receptor (PR), and HER2, combined with patient and pathological variables such as age, tumor size, tumor grade, and node involvement[13, 14]. Despite the prognostic power of classic IHC markers, the vast number of genes that can contribute to cell proliferation means that these markers can become limited in advanced settings. In 2000, Perou *et al*. used a genome wide (~8,000 genes) microarray to first define the four major intrinsic subtypes of breast cancer: Luminal A, Luminal B, HER2 positive, and Basal [15] (later refined with an expanded cohort[16]).

These four subtypes were distilled into a 50 gene classifier, termed the PAM50[17], that has demonstrated prognostic value[18]. NanoString utilized this PAM50 signature to develop a clinical prognostic assay to predict the likelihood of recurrence, Prosigna™[19], that was granted FDA approval in 2013. This inspired the development of additional prognostic gene signature assays, OncoType DX™[20] and MammaPrint™[21], that can help clinicians identify patients that can safely forego adjuvant chemotherapy.

1.3 Treatment Options in Breast Cancer

Ultimately, all treatment decisions are made on an individual basis by physicians and patients. However, front-line therapy remains highly consistent across the major intrinsic subtypes. Surgery and radiotherapy are utilized across all subtypes. ER positive tumors are offered endocrine therapy, either in the form of an ER targeting agent (such as tamoxifen or fulvestrant) or an aromatase inhibitor (such as letrozole)[22]. ER targeting agents that act as competitive antagonists are termed Selective Estrogen Receptor Modulators (SERMs), while agents that bind to ER destabilizing the

protein, preventing dimerization, and ultimately leading to protein degradation are referred to as Selective Estrogen Receptor Degraders (SERDs). Aromatase inhibitors, which are generally offered for post-menopausal women, inhibit the enzyme aromatase (also known as estrogen synthase) in periphery organs, the enzyme responsible for the vast majority of estrogen production in post-menopausal women[23]. HER2 positive tumors are offered a HER2 targeted therapies, most commonly trastuzumab[24]. Patients with basal (commonly referred to as triple negative) disease are uniformly given chemotherapy. Patients with 'high risk' ER and HER2 positive disease are also commonly given chemotherapy to reduce the chance of recurrence[25].

1.4 Therapy Resistance

While ER and HER2 targeted therapies have dramatically improved patient care, approximately 25% of all BrCa patients will eventually relapse, with acquired therapy resistance posing a major clinical challenge[26]. Roughly 25% of patients with primary ER-positive disease, and nearly all of those with metastatic disease will eventually develop endocrine therapy resistance[26]. Recent studies have highlighted activating mutations in the ligand binding domain of *ESR1* as a common mechanism of therapy resistance. Occurring in roughly 20% of metastatic ER positive tumors, these mutations are believed to confer ligand independent activity[27]. Amplifications in other growth factor receptors including *FGFRs* and *ERBBs* have been shown to replace the functional loss of ER expression, helping to maintain activation of mitogenic pathways such as Pi3K/AKT and MAPK/ERK[28-30]. Similar resistance mechanisms exist for HER2 targeted therapies. A truncated isoform of HER2 has been shown to confer resistance to trastuzumab, while gatekeeper mutations have been proposed to reduce the efficacy of small molecule HER2 inhibitors[31, 32].

1.5 Mutational Landscape in Primary and Metastatic Breast Cancer

Large-scale sequencing and microarray studies from The Cancer Genome Atlas (TCGA[33]) and the Molecular Taxonomy of Breast Cancer International Consortium (METABRIC[34]) have helped to shed light onto just how incredibly complex and heterogeneous cancers are, and helped to identify novel genetic drivers. However, recurrent point mutations in BrCa are rare, with only *TP53*, *PI3KCA*, and *GATA3* being mutated in more than 10% of primary tumor samples[35]. Few studies have found specific patterns of mutations within the major subtypes of BrCa. For example, ER positive tumors are often found to have activating mutation in the PI3K/AKT pathway and inactivation of *GATA3* and the *JUN* pathway. Triple negative tumors most often present with *TP53* mutations, and extensive copy-number variation[35].

With such few recurrent mechanisms of therapy resistance, screening tumors for genomic drivers with sequencing-based assays has become more and more routine, helping to match patients with targeted therapy clinical trials. Independent of the previously described expression-based prognostics, companies and university labs have also begun to develop targeted DNA sequencing panels to identify pathological driver mutations. Two mutation profiling panels that can be used to help oncologist match patients with clinical trials, the Memorial Sloan Kettering – Integrated Mutational Profiling of Actionable Cancer Targets[36] (MSK-IMPACT™) and the Foundation Medicine - Foundation ONE™[37], have recently been granted FDA approval.

1.6 Breast Cancer Recurrence and Metastasis

Much of the success of novel therapies in cancer can be attributed to an increase in the understanding in the biology of the disease. While survival rates for primary BrCa have continued to improve over the past 5 years, prognosis for women diagnosed with recurrent or metastatic disease has remained bleak (5yr survival of ~25%)[38]. Approximately 10-15% of patients

diagnosed with BrCa will develop a distant metastasis within 3 years of the initial diagnosis[39]. That said, recurrent metastatic lesions appearing 10 or more years after initial diagnosis is not uncommon either, meaning women in remission are never true free of the burden of potential relapse.

Breast cancers can reoccur locally, within the breast tissue or chest wall, or at distant metastatic sites. The most common sites of distant metastasis for breast cancer are bone, liver, lung and brain [39]. Metastasis is a multistep process that includes acquiring an aggressive self-renewing phenotype, detachment from the extracellular matrix, invasion into surrounding tissue, penetrating into and surviving the mechanical stresses in circulation, lodging into the capillaries of a secondary organ, extravasation out of the blood stream, and overt colonization in a novel microenvironment, all the while fending off the immune system and systemic therapies[40, 41]. Metastatic lesions can then repeat the entire process, leading to further diversification of cells and tumors. The final step in this process, colonization, represents the single greatest challenge for cancer cells, as the vast majority will undergo apoptosis when exposed to paracrine and juxtracrine signaling in a novel microenvironment. An estimated 0.01-0.02% of disseminated cancer cells are able to successfully generate a metastatic lesion[42].

1.7 Metastatic Tropism

Given the extensive body of evidence showing the dynamic interactions between cancer cells and the surrounding microenvironment, it is no surprise that certain genetic features can ‘prime’ cells for colonization in specific distant organs (Briefly reviewed [43]). This is the basis of the “Seed and soil” hypothesis, originally proposed by Stephen Paget in 1889[44]. To date, the dynamics that mediate metastatic tropism are largely unknown.

Perhaps the greatest piece of evidence for the seed and soil hypothesis is the dramatically different pattern of metastasis among cancer types. Nearly 50% of patients with metastatic lung cancer will develop brain metastases, compared to roughly 25% for BrCa patients and just below 20% for melanoma patients[1, 45]. Meanwhile, other common malignancies such as thyroid, gastrointestinal, and prostate cancer rarely ever form metastases in the central nervous system[46].

In an attempt to identify genes that mediate BrCa brain metastasis, Bos *et al*. [47]performed comparative genome-wide expression analysis on parental, and matched brain homing cell line variants. They identified COX2, HB-EGF, and ST6GALNAC5 as important mediators of extravasation through the blood brain barrier. Lee *et al*.[48] used an in *vitro* blood brain barrier model to show that CXCL12-CXCR4 signaling promoted MDA-MB-231 transendothelial migration through a monolayer of human brain microvascular endothelial cells. Multiple independent studies have shown that *ERBB2* overexpression and *PTEN* loss are positively selected for in patient matched brain metastases[49, 50]. Multiple studies have also highlighted the importance of HER3, HER2-HER3 heterodimerization and the PI3K/AKT pathway in the formation of therapy resistant brain metastases [51-53].

In the next chapter, I describe the development and validation of MammaSeq, a targeted sequencing panel designed based on current knowledge of the most common, impactful, and targetable drivers of metastatic breast cancer. Through the validation of MammaSeq, we identified several *RET* mutations that, bioinformatically, appear as though they may play a functional role in tumorigenesis. In two other recently completed studies from the Lee Lab, RET appeared as a potential mediator of BrCa brain metastasis. In chapter 2, I investigate the hypothesis that the overexpression of RET, facilitates BrCa brain metastasis, due to the high levels of the RET ligand, GDNF, in the brain microenvironment.

2.0 TARGETED MUTATION DETECTION IN ADVANCED BREAST CANCER USING MAMMASEQ

*This chapter is an amended version of our previous publication[54].

2.1 BACKGROUND

Advanced breast cancer is currently incurable. Selection of systematic therapies is primarily based on clinical and histological features and molecular subtype, as defined by clinical assays[55]. Large-scale genomic studies have shed light into the heterogeneity of breast cancer and its evolution to advanced disease[35, 56], and coupled with the rapid advancement of targeted therapies, highlights the need for more sophisticated diagnostics in cancer management[57]. Next-generation sequencing (NGS) based diagnostics allow clinicians to identify specific putative driver events in individual tumors. Correctly identifying disease drivers may enable clinicians to better predict treatment responses, and significantly improve patient care[58]. However, to date, the use of NGS in clinical diagnostics remains limited[59]. Published data regarding prognostic utility, and utilization for selection of targeted therapies or enrolment in clinical trials is far from comprehensive.

The AmpliSeq Cancer Hotspot Panel (ThermoFisher Scientific) was shown to have a diagnostic suitability in primary lung, colon, and pancreatic cancers[60], however, our previous report that surveyed the clinical usefulness of the 50 gene AmpliSeq Cancer Hotspot Panel V2 in breast cancer found that the panel lacked numerous key known drivers of advanced breast cancer[61]. For example, the panel does not include any amplicons in *ESR1*, which harbor mutations which are known to contribute to hormone therapy resistance (for review see[26]), and lacks coverage of the majority of known driver mutations in *ERBBB*[62].

The lack of any reported breast cancer specific diagnostic NGS test inspired the development of MammaSeq^{TM}, an amplicon based NGS panel built specifically for use in advanced breast cancer. 46 solid tumor samples from women with advanced breast cancer, plus an additional 14 samples of circulating-free DNA (cfDNA) from patients with metastatic breast cancer were used in this pilot study to define the clinical utility of the panel. The patient cohort encompassed all 3 major molecular subtypes of breast cancer (luminal, HER2 positive and triple negative), and both lobular and ductal carcinomas (Table 1).

Table 1: Patient and Specimen Characteristics.

	Patients with available tumor tissue (n=46)
Age	
Median age (yrs)	45
Range (yrs)	31-71
Race	
White	45 (97.8%)
Black	1 (2.2%)
Site	
Primary	10 (21.7%)
Metastatic	36 (78.3%)
Stage (Dx)	
I	10 (21.7%)
II	8 (17.4%)
III	13 (28.3%)
IV	4 (8.7%)
Unknown	11 (23.9%)
Hormone-receptor	
HR + and HER2 –	19 (41.3%)
HR + and HER2 +	5 (10.9%)
HR + and HER2 Unknown	1 (2.2%)
HR – and HER2 +	1 (2.2%)
HR – and HER2 –	17 (36.9%)
Both Unknown	2 (4.3%)
Histopathology	
Ductal	34 (73.9%)
Lobular	5 (10.9%)
Mixed	3 (6.5%%)
Other/Unknown	4 (8.7%)

2.2 MATERIALS AND METHODS:

2.2.1 Patient Sample Collection

For MammaSeq NGS testing, this study utilized breast tumors from 46 patients and blood samples from 7 patients. The research was performed under the University of Pittsburgh IRB approved protocol PRO16030066. The general patient characteristics are shown in Table 1 and more detailed patient information is shown in Table 4. We utilized 46 of the 48 breast cancer cases previously described in a report by Gurda *et al*.[63]. All of these cases previously underwent AmpliSeq Cancer Hotspot Panel V2 (ThermoFisher Scientific) NGS testing between January 1, 2013 and March 31, 2015 within the UPMC health system. MammaSeq was performed on the identical genomic DNA isolated from these tumor specimens that was originally used for initial clinical testing. 2 cases were excluded due to insufficient DNA. In addition, a cohort of 7 patients with metastatic breast cancer (MBC) had 20ml venous blood drawn in Streck Cell-Free DNA tubes between July 1, 2014 and March 29, 2016. All patients signed informed consent, and samples were acquired under the University of Pittsburgh IRB approved protocol (IRB0502025). We previously reported on the detection of ESR1 mutations in cfDNA from these 7 patients using ddPCR[64]. Serial blood draws (range; 2-5) were available for 4 patients. A total of 14 blood samples from 7 patients were utilized for cfDNA, buffy coat DNA isolation, and NGS testing followed by ddPCR.

2.2.2 Patient Sample Processing

cfDNA was isolated as described previously[64]. Blood was processed to separate plasma and buffy coat by double centrifugation within 4 days of blood collection. 1ml to 4ml of plasma was used for isolation of cfDNA using QIAamp Circulating Nucleic Acid kit (Qiagen). cfDNA was quantified using Qubit dsDNA HS assay kit (ThermoFisher Scientific). Genomic DNA was isolated from buffy coat using DNeasy Blood & Tissue Kit (Qiagen) for use as germline DNA

control. Buffy coat DNA was quantified using Qubit dsDNA BR assay kit (ThermoFisher Scientific).

2.2.3 Ion Torrent Sequencing

20ng of DNA (10ng per amplicon pool) was used for library preparation using Ion AmpliSeq™ Library Kit 2.0 (Thermo Fisher Scientific) and the custom designed MammaSeq primer panel (Supplementary Data File 1). Template preparation by emulsion PCR and enrichment was performed on the Ion OneTouch 2 system (ThermoFisher Scientific). Template positive Ion Sphere particles (ISP) were loaded onto Ion chips and sequenced. Tumor DNA and cfDNA samples were sequenced using P1 chips (60 million reads) on the Ion Proton™ (ThermoFisher Scientific) at empirical depths of 1000x and 5000x respectively. Buffy coat DNA was sequenced using a 318 chip (6 million reads) on the Ion Torrent Personal Genome Machine (PGM™, ThermoFisher Scientific) at 500x (Sequencing done by the University of Pittsburgh Health Sciences Genome Research Core).

2.2.4 Variant Calling

Ion Torrent Suite V4.0 was used to align raw fastq files to the hg19 reference genome and generate VCF files (4.0% AF cutoff for tumor samples, 1.0% AF cutoff for cfDNA samples). Cravat CHASM-v4.3 (http://hg19.cravat.us/CRAVAT/) was used to annotate variants with resulting protein changes and snp annotation from ExAC[65] and 1000Genomes[66]. Variant calls from buffy coat DNA were used to remove germline variants from the 14 cfDNA samples in a patient matched manner. SNP and sequencing artifact filtering, data organization, and figure preparation were performed in R (v3.4.2). The R package ComplexHeatmaps was used to generate figures 1 and 3A[67]. CNVKit was used to call copy number across all genes, however only genes containing more than 3 amplicons were reported (Table 2)[68]. DNA from the buffy coat of the

cfDNA cohort was used to generate a single copy-number reference which was used as a baseline for copy number calling on the solid tumor cohort. CNKit reports copy number as a log2 ratio change. CNV were reported if the absolute copy number was above 6 (log2(6/2)=1.58) or below 1 (log2(1/2) = -1).

2.2.5 Data and code

Annotated, unfiltered, mutation and CNV data, along with R code related to this study, are deposited on GitHub. (https://github.com/smithng1215)

2.2.6 Droplet-Digital PCR

2 ng of cfDNA or buffy coat DNA was subjected to targeted high-fidelity preamplification for 15 cycles using custom designed primers (Table 5) and PCR conditions previously described[64]. Targeted preamplification products were purified using QIAquick PCR Purification kit (Qiagen) and diluted at 1:20 before use in ddPCR reaction. 1.5ul of diluted preamplified DNA was used as input for ddPCR reaction. ddPCR was performed for ESR1-D538G, FOXA1-Y175C, and PIK3CA-H1047R mutations. Custom ddPCR assays were developed for ESR1-D538G (Integrated DNA Technologies) and FOXA1-Y175C (ThermoFisher Scientific). Sequences are described in Table 6. PIK3CA-H1047R was analyzed using PrimePCR ddPCR assay (Bio-Rad Laboratories) dHsaCP2000078 (PIK3CA)/ dHsaCP2000077 (H1047R). Nuclease-free water and buffy coat-derived wildtype genomic DNA as negative controls, and oligonucleotides carrying mutation of interest or DNA from a cell line with mutation as positive controls were included in each run to eliminate potential false positive mutant signals. An allele frequency of 0.1% was used as a lower limit of detection.

2.2.7 Statistical Analysis

All statistical analysis was performed in R 3.4.2. To determine if there was a significant correlation between mutational burden and copy number burden, we calculated the Pearson correlation coefficient between the number of somatic mutations in each sample, with the number of significant copy number changes in each sample.

2.3 RESULTS

2.3.1 Development of MammaSeq Panel

To build a comprehensive list of somatic mutations in breast cancer, Drs. Hartmaier and Bahreini (from the Lee-Oesterreich lab) combined mutation calls from primary tumors in TCGA (curated list level 2.1.0.0) and limited studies focused on metastatic breast cancer [69-71]. The biological function and druggablity of mutated genes were investigated via Gene Ontology (GO) [72] and DGIdb (v2.0) databases [73]. The information regarding FDA approved drugs was downloaded from "https://www.fda.gov/Drugs" and added to our list. We used the following criteria to prioritize the clinically important mutated genes:

- The mutated gene is among significantly mutated genes (SMGs) in primary and metastatic samples.
- The mutated gene is clinically actionable (e.g. there is available FDA-approved drug(s) against it).
- The mutated gene is of functional importance in cancer (e.g. kinase genes were scored higher in the list).
- The mutation has been found in more than 5 primary tumors OR 2 metastatic tumors.
- The mutation has been found in both primary and metastatic lesions.

The final mutation list was then curated and narrowed down to 80 genes and 1398 mutations. Additional amplicons were added to select genes to ensure sufficient coverage of genes known to harbor functional copy-number variants. Amplicon probe design was unsuccessful for 29 mutations, including all 3 mutations in the gene HLA-A, yielding a final panel consisting of 688 amplicons targeting 1369 mutations across 79 genes. (Selected genes described in Table 2. Gene coverage depicted in Figure 12).

The panel includes 34 of the 50 (68%) genes incorporated in AmpliSeq Cancer Hotspot Panel V2. Genes that were not mutated in breast cancer (TCGA and in-house data) and genes that were not considered to be clinically actionable were not included. The MammaSeq panel includes 8 of the 10 (80%) genes and ~ 91% of the hotspots targeted by the Thermo Oncomine Breast cfDNA assay. MammaSeq covers 14% of the base pairs covered by the Qiagen Human Breast Cancer GeneRead DNAseq Targeted Array, however, it covers hotspots in over half of the genes (57%, plus an additional 34 genes). Of these panels, MammaSeq is the only one that includes

Table 2: Genes Incorporated in the MammaSeq Panel

ABL1	CDK6	FGFR3	KDR	NOTCH1
AKT1	CDKN1B	FGFR4	KIT	NRAS
AKT3	CDKN2A	FOXA1	KMT2C	PAK1
ALK	CDKN2B	GATA3	KRAS*	PDGFRA
AR	CTCF	GRB7	MAP2K4	PIK3CA
ARID1A	CTNNB1	HIST2H2BE*	MAP3K1	PIK3R1
ATM	DNAH14	HRAS*	MAP3K4	PTCH1
AURKA	EGFR	IDH1*	MDM2	PTEN
AURKB	ERBB2	IGF1R	MDM4	RB1
BRAF	ERBB3	IKBKB	MET	RET
BRCA1	ERBB4	IKBKE	MTOR	RPTOR
BRCA2	ESR1	INPP4B	MYC	RUNX1
CCND1	EZH2*	INSR	NCOA3	SMO
CCNE1	FGF19	JAK2	NCOR1	STK11
CDH1	FGFR1	JAK3	NCOR2	TP53
CDK4	FGFR2	JUN*	NF1	

* denotes genes with less than 3 amplicons, for which copy number changes were not reported

CDK4 and CDK6, both of which can be targeted with FDA approved CDK4/6 inhibitors [74]. Additional genes unique to MammaSeq include common drivers, CCND1, MTOR, and FGFR4. Finally, MammaSeq covers 68 of 315 genes targeted by the larger pan cancer Foundation Medicine, FoundationOne panel. Figure 13 details the overlap in coverage between MammaSeq and above mentioned commercially available panels.

2.3.2 Characterization of Genetic Variants detected by MammaSeq in a Solid Tumor Cohort

To evaluate performance in mutation detection by the MammaSeq panel, sequencing was carried out on a cohort of 46 solid tumor samples, with a mean read depth of 2311X (Figure 14). 4970 total variants (mean: 106, median: 82) were called across all patient samples. I removed identical genomic variants that were present in more than 10 samples as these were likely to be sequencing artifacts or common SNPs. Removing non-coding and synonymous variants yielded 1433 and 901 variants, respectively. To filter out less common polymorphisms, I removed variants annotated in ExAC [65] or the 1000Genomes [66] databases in more than 1% of the population. I removed variants with an allele frequency above 90%, as these were likely germline. Finally, to focus on high confidence mutations, I removed variants with a strand bias outside of the range of 0.5-0.6, yielding a total of 592 protein coding mutations (mean 12.9, median 3, IQR 3) (Figure 1).

Interestingly, as noted by the variation between the mean and median, the total number of mutations was skewed toward a subset of samples (Figure 1-top panel). 408 of the 592 mutations (69%) were found in just 4 of the 46 samples (Figure 15). These 4 samples are outliers, as they are all more than 1.5 times the IQR plus the median. 3 of these 4 samples with high mutational burden were of triple negative subtype, while the fourth was $ER^{+}/HER2^{+}$. The most common mutated genes were *TP53* (57%) and *PIK3CA* (43%). We also noted common mutations in *ESR1* (21%),

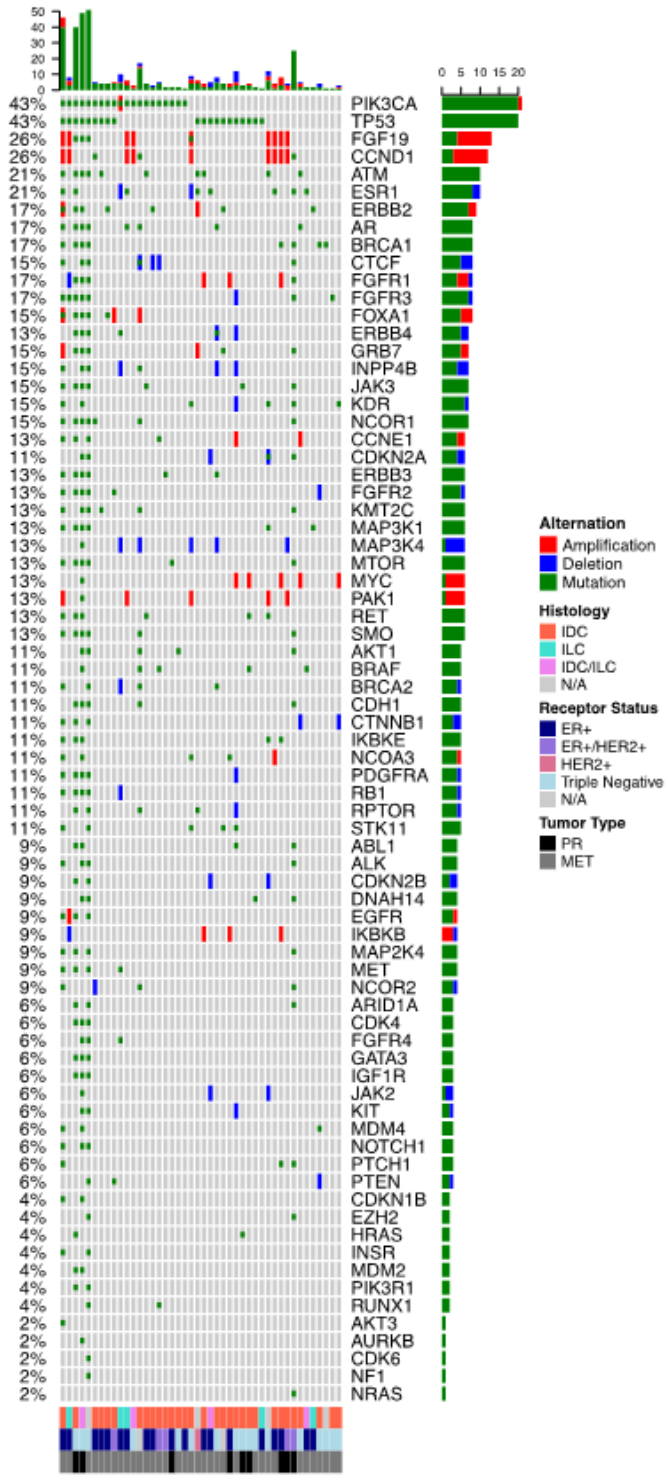

Figure 1: Genetic alterations identified by the MammaSeq gene panel in a test cohort of 46 breast cancers.

Oncoprint depicting the distribution of somatic mutations, copy-number amplifications (absolute copy-number greater that 6) and deletions (absolute copy-number less than 1).

ATM (21%) and *ERBB2* (17%).

To examine changes in CNV, we established a baseline for pull down and amplification efficiency by performing MammaSeq on normal germline DNA from 14 samples (7 patients – 6 additional). CNVkit [68] was used to pool the normal samples into single reference and then call CNV in the solid tumor cohort (Figure 1). CNV were identified in many common oncogenes including *CCND1*, *MYC*, *FGFR1* and others. 2 of the 3 *ERBB2*$^{+}$ samples (via clinical assay) showed CNV by MammaSeq. *FGF19* and *CCND1* were co-amplified in 9 of the 46 (20%) solid tumors. Both genes are located on 11q13, a band identified in GWAS as harboring variants, including amplifications, associated with ER^{+} breast cancers [75]. There wasn't a correlation between mutational burden and copy number burden (Pearson correlation p-value = 0.7445).

2.3.3 Clinical Utility of Genetic Variants Detected by MammaSeq

To determine how many of the mutations have putative clinical utility, I utilized the OncoKB precision oncology knowledge database [76]. 25 of the genes in the MammaSeq panel (32% of the panel) harbor clinically actionable variants with supporting clinical evidence (OncoKB levels 1-3). In total, I identified 28 actionable variants (26 SNV and 2 ERBB2 amplifications) that have supporting clinical evidence (level 1-3) and an additional 3 actionable variants supported by substantial research evidence (level 4) in the solid tumor cohort (Table 3). The 26 SNVs were distributed across 20 of the 46 cases (43%) (Figure 2). Consistent with the report detailing the development of the OncoKB database [36], the vast majority of actionable variants in breast cancer are annotated at level 3, indicating that variants have been used as biomarkers in clinical trials, however they are not FDA approved. In fact, the only level 1 annotated variant in breast cancer is *ERBB2* amplification.

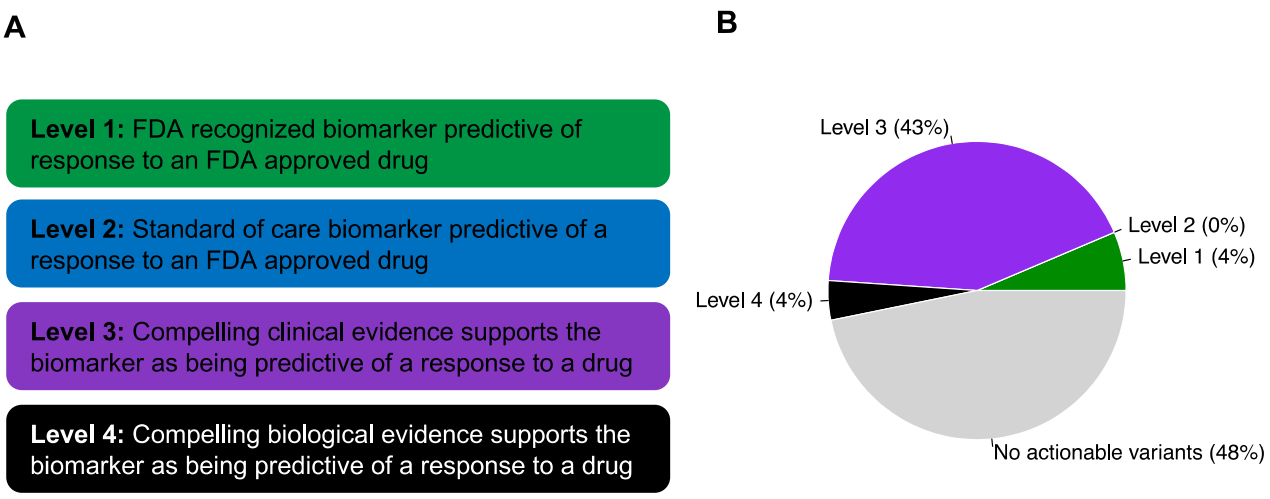

Figure 2: Clinical actionability of MammaSeq identified somatic alterations.
(A) Annotation levels, adapted from OncoKB **(B)** Samples were categorized based on the most actionable alteration. Specific alterations and associated drugs are depicted in Table 3.

2.3.4 Characterization of Genetic Variants detected by MammaSeq in cfDNA

To examine the potential of MammaSeq to detect variants in cfDNA, we sequenced 14 cfDNA samples isolated from 7 patients with metastatic disease (originally obtained by Rekha Gyanchandani a postdoc in the Lee lab). cfDNA samples were sequenced to a mean depth of 1810X, while matched buffy coat gDNA was sequenced to a mean depth of 425X (Figure 15). We applied the same filtering pipeline to the cfDNA variants and solid tumor variants, except in the smaller cohort I removed all identical variants found in more than 4 samples, and lowered the minimum allele frequency to 1.0%. I identified a total of 43 somatic mutations across the 14 cfDNA samples (mean: 3.1, median 1, IQR 1.75) (Figure 3A). Like the solid tumor cohort, a single draw from 1 patient (CF_28-Draw 1) harbored 13 of the 25 (58%) total mutations. Using the same definition, this sample is also an outlier. Similar to the solid tumor cohort, *PIK3CA* and *ESR1* were among the most commonly mutated genes.

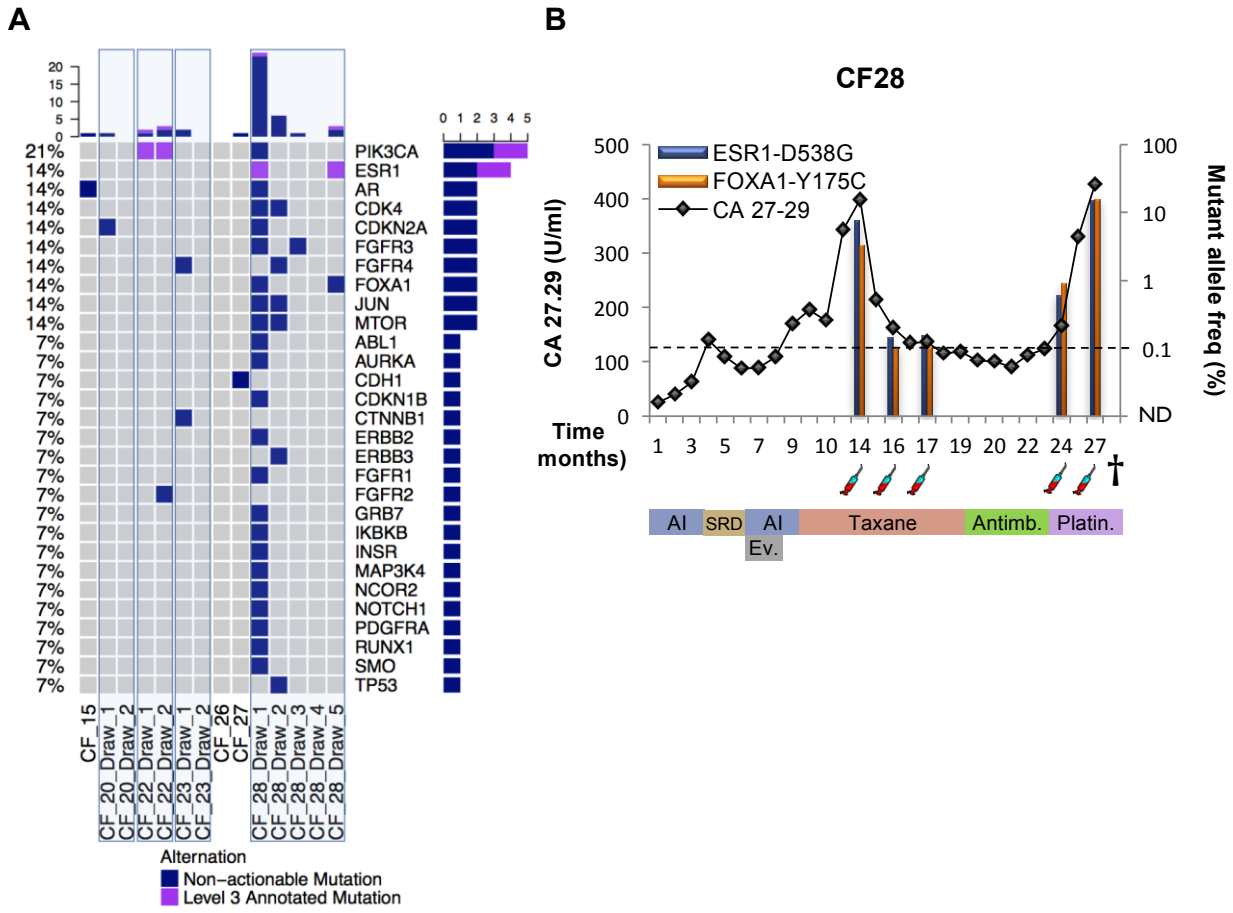

Figure 3: Genetic alterations identified by MammaSeq in cfDNA from a test cohort of 7 patients with metastatic invasive ductal carcinoma.
(A) Oncoprint of somatic mutations identified in 14 cfDNA samples. **(B)** Clinical timeline and mutant allele frequency of ESR1-D538G and FOXA1-Y175C mutations in serial blood draws from patient CF28. The timeline starts with diagnosis of metastasis and shows tumor marker assessments (CA 27.29 antigen line graph), mutant allele frequency (bar graphs), LLoD (dotted line), blood draws (syringe), and treatments received. Treatment abbreviations: AI (aromatase inhibitor), SERD (selective estrogen receptor degrader), Ev. (Everolimus), Antimb. (Antimetabolite), Platin (Platinum-based chemotherapy).

Two of the identified somatic mutations (each identified in 2 draws from 1 patient) are annotated at level 3 in the OncoKB database, ESR1 - D538G and PIK3CA - H1047R (Figure 3A). The *ESR1* mutation was identified in 2 separate blood draws from patient CF_28 taken 13 months apart. Interestingly, the FOXA1 – Y175C mutation was also identified in the same draws from

patient CF_28 (Figure 3B). The allele frequencies of these mutations strongly correlate with levels of cancer antigen 27-29 (CA-27.29), indicating that the mutation frequencies are likely an indicator of disease burden. Mutations identified in all three genes (ESR1, PIK3CA, and FOXA1) were independently validated using ddPCR (ddPCR validation done by Rekha Gyanchandani) (Figure 16).

2.3.5 *RET* mutations identified in the MammaSeq Cohort

We identified 4 novel mutations in the kinase domain of RET, all of which are predicted to be pathogenic (Cravat CHASM $p<0.05$[77]); G825D, D842N, S891L, and M918I (Figure 4A). In fact, the mutations S891L and M918I affect residues that are known to cause multiple endocrine neoplasia (MEN2) type-2a (891) and type-2b (918)[78]. Studies have shown that mutations at these residues induce ligand and co-receptor independent activation of monomeric RET molecules[79]. G825D and D842N are novel mutations, unannotated in databases such as COSMIC[80], however the elevated allele frequencies (4.3 and 3.1% respectively) in metastatic samples suggest these mutations may be functioning as tumor drivers.

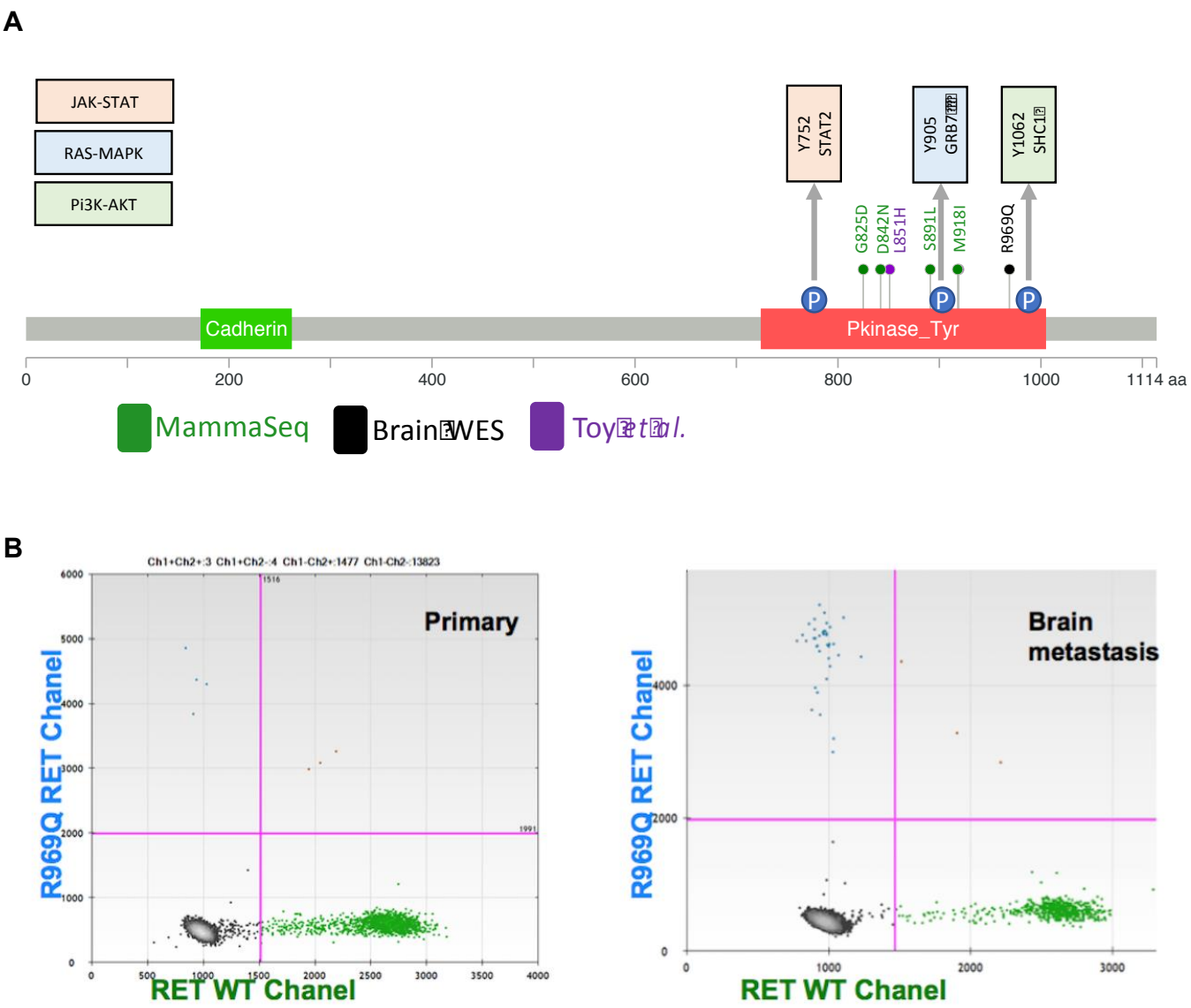

Figure 4: RET mutations identified in 3 independent cohorts of advanced breast tumors. **(A)** Lollipop plot (cBioPortal.org) of the 4 pathogenic variants identified in the MammaSeq cohort, 2 variants from previously published studies, and 1 variant from the patient matched whole exome sequencing cohort. **(B)** ddPCR validation of the mutation allele frequency of RET R969Q in the primary tumor (left – 0.45%) and matched brain metastasis (right -6.6%). (WES study and ddPCR validation done by Ryan Hartmaier and Yijing Chen)

Table 3: Identified variants annotated in OncoKB with corresponding targeted therapeutics.

Sample ID	Gene	Protein Sequence Change	Allele Frequency	Level	Drugs
MET_03	ERBB2	Amplification	-	1	Lapatinib + Trastuzumab, Pertuzumab + Trastuzumab, Ado-trastuzumab emtansine, Lapatinib, Trastuzumab
MET_33	ERBB2	Amplification	-	1	
MET_39	AKT1	E17K	0.25	3	AZD5363
MET_18	ERBB2	I654V	0.122222	3	Neratinib
MET_32	ERBB2	I654V	0.461731	3	
MET_49	ERBB2	I654V	0.495495	3	
MET_07	ESR1	D538G	0.477717	3	AZD9496, Fulvestrant
MET_21	ESR1	D538G	0.335884	3	
MET_28	ESR1	D538G	0.454271	3	
MET_27	ESR1	Y537S	0.376441	3	
MET_22	PIK3CA	E453K	0.444722	3	Buparlisib, Serabelisib, Alpelisib + Fulvestrant, Copanlisib, GDC-0077, Alpelisib, Taselisib + Fulvestrant, Buparlisib + Fulvestrant, Taselisib
MET_10	PIK3CA	E542K	0.106212	3	
MET_21	PIK3CA	E542K	0.501912	3	
MET_41	PIK3CA	E542K	0.073183	3	
MET_49	PIK3CA	E542K	0.467702	3	
MET_08	PIK3CA	E545K	0.204327	3	
MET_34	PIK3CA	E545K	0.0871914	3	
MET_40	PIK3CA	E545K	0.844344	3	
MET_25	PIK3CA	H1047R	0.341171	3	
MET_29	PIK3CA	H1047R	0.180681	3	
MET_32	PIK3CA	H1047R	0.2785	3	
MET_33	PIK3CA	H1047R	0.413998	3	
MET_38	PIK3CA	H1047R	0.384692	3	
MET_44	PIK3CA	H1047R	0.60054	3	
MET_06	PIK3CA	N345K	0.376571	3	
MET_35	PIK3CA	Q546R	0.435484	3	
PR_26	BRAF	G469A	0.52028	4	LTT462, BVD-523, KO-994
MET_34	KRAS	G12D	0.074	4	LY3214996, KO-947, GDC-1014
MET_22	PTEN	C136Y	0.756233	4	AZD6482 + Alpelisib
CF_28_Draw_1	ESR1	D538G	0.0746562	3	AZD9496, Fulvestrant
CF_28_Draw_5	ESR1	D538G	0.146853	3	
CF_22_Draw_1	PIK3CA	H1047R	0.320088	3	Buparlisib, Serabelisib, Alpelisib + Fulvestrant, Copanlisib, GDC-0077, Alpelisib, Taselisib + Fulvestrant, Buparlisib + Fulvestrant, Taselisib
CF_22_Draw_2	PIK3CA	H1047R	0.402402	3	

2.4 DISCUSSION

Advances in the accuracy, cost, and analysis of NGS make it an ideal platform to develop diagnostics that can be used to precisely identify treatment options. MammaSeq was developed to comprehensively cover known driver mutation hotspots specifically in primary and metastatic breast cancer that would identify mutations with potential prognostic value. Typically, NGS diagnostics are reserved for late stage disease. As a result, the solid tumor cohort was significantly enriched for metastatic disease and markers of poor prognosis - triple negative subtype, late presentation, and therapy resistance.[61]

Consistent with previous mutational studies, we report that a small subset of breast cancers harbor high mutational burden.[81] Across a variety of cancers, groups have demonstrated the correlation between the tumor mutation burden (TMB) and the efficacy of immunotherapy checkpoint inhibitors (reviewed here[82]). However, the ability to accurately depict tumor mutation burden is dependent on the percentage of the covered exome. Illumina have shown that the TruSight Tumor 170 panel (170 genes and 0.524 Mb) begins to skew the TMB upwards, when used on samples that contain relatively few mutations [83]. Similarly, a study by Chalmers *et al*. used a computational model to show that below 0.5Mb, TMB measurements are highly variable and unreliable [84]. The MammaSeq panel covers just 82,035bp (0.08Mb), and therefore likely cannot be used to calculate a mutational burden comparable to whole exome based studies. That being said, the stark difference in the total number of mutations identified in the subset of 4 tumor samples, suggests a high TMB, meaning these patients may be suited for immunotherapy.

Liquid biopsies are beginning to be utilized clinically after numerous proof-of-principle studies have demonstrated the potential of circulating cell-free DNA (cfDNA) for prognostication, molecular profiling, and monitoring disease burden [64, 85-89]. We have demonstrated that the

MammaSeq panel can be used to identify mutations in cfDNA. For one patient (CF_28), we have cfDNA data from 5 blood draws taken over the course of 13 months. The sharp drop-off in the number of somatic mutations identified between the first and second draws co-occurs with a decrease in CA.27.29 levels, suggesting that the patient may have responded well to treatment, leading to disappearance of sensitive clones. In the later blood draws, we did not observe an increase in the total number of somatic mutations, but instead an increase in the allele frequency of ESR1-D538G and FOXA1-Y175C mutations, which may be caused by therapeutic selection of resistant clones.

High-throughput genotyping of solid tumors and continual monitoring of disease burden through sequencing of cfDNA represent potential clinical applications for NGS technologies. It should be noted that targeted DNA sequencing panels such as MammaSeq are far less comprehensive than whole exome sequencing and they do not allow for evaluation of structural variants, which may lead to gene fusions that function as drivers [90]. Nevertheless, as focused panels represent cost-effective and useful alternatives to whole exome sequencing for targeted mutation detection. This data provides further evidence for the use of NGS diagnostics in the management of advanced breast cancers.

3.0 INVESTIGATING THE ROLE OF RET IN BREAST CANCER METASTASIS

3.1 BACKGROUND

The Lee-Oesterreich Lab recently reported in *JAMA Onc* that brain metastases undergo molecular evolution, with intrinsic subtype switching and a gain of ERBB2 amplification[91]. The lab has now completed an unbiased study using RNA exome sequencing of 45 patient-matched pairs of primary and metastatic breast cancers from 4 different recurrence sites (21 brain, 11 bone, 3 gastrointestinal and 10 ovary). Nolan Priedigkeit performed all sample preparation and sequencing analysis pertaining to the brain cohort. He focused the analysis on metastatic expression gains, in clinically actionable kinases. RET was among the most recurrently upregulated kinases in the brain metastasis cohort, with expression gains (defined as the top 5% of genes after ranking by fold-change) in 8 of the 21 pairs (38%) (Figure 5). Notably, RET was not increased at other metastatic sites.

The ligands for RET, a transmembrane receptor tyrosine kinase (RTK), are the glial cell-line derived neurotrophic factors (GDNFs), which are expressed almost exclusively in the central nervous system[92]. GDNFs bind to a family of co-receptors, termed glial cell-line derived neurotrophic factor receptors (GFRs)[93], and facilitate RET heterodimerization. Dimerization initiates auto-phosphorylation on several intracellular cysteine residues[94]. The phosphorylated residues then function as docking sites for PTB and SH2 domain-containing proteins such as STAT3, SRC, and GRB family proteins, among others, which further transduce the receptor signal[79, 95]. Functionally, RET is known to play a vital role in the development and homeostasis of neurons and aberrant activation of RET signaling is a known driver of other cancers such as

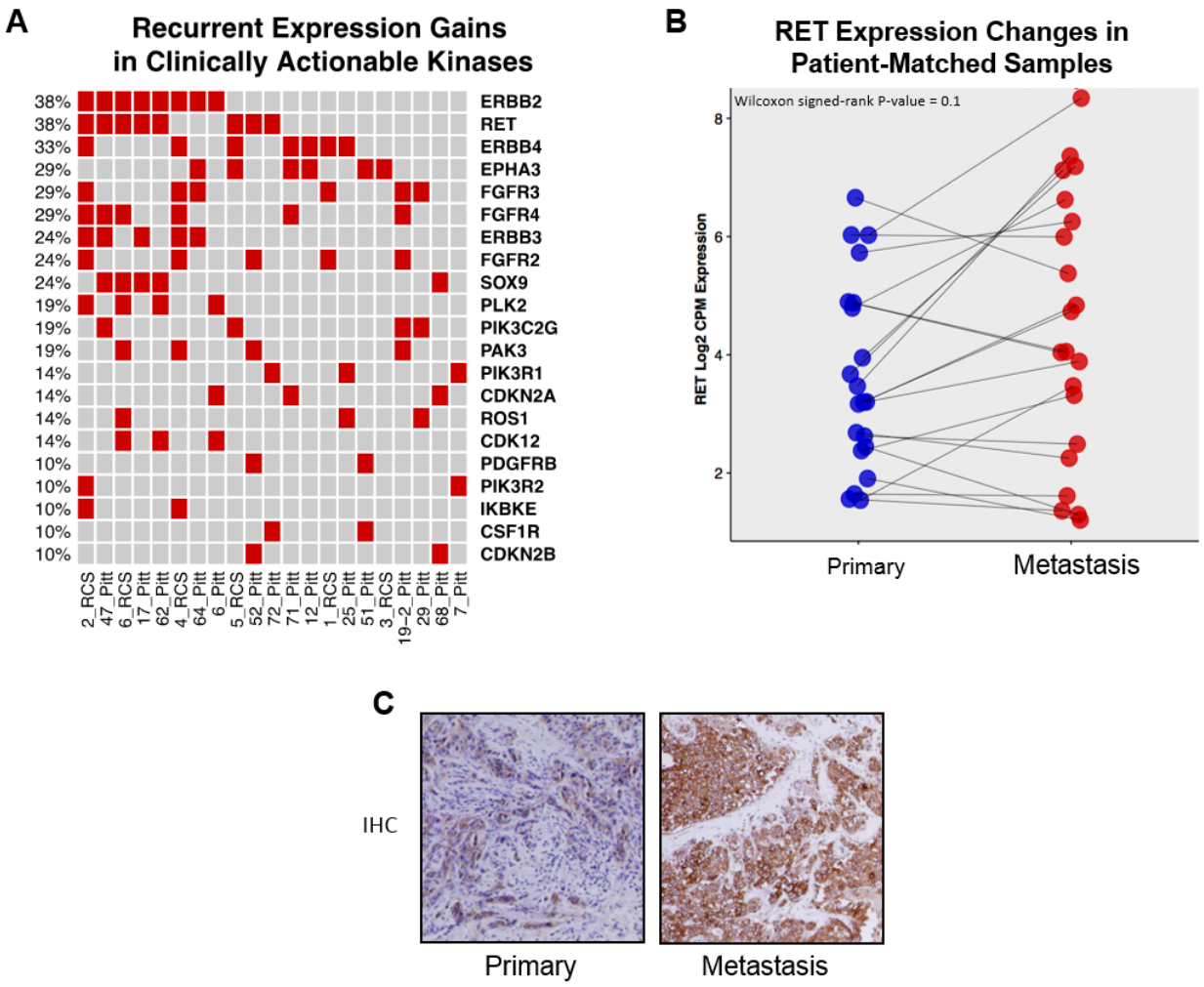

Figure 5: Recurrent RET expression gains in breast cancer brain metastasis.
(A) Oncoprint of expression gains in clinically actionable kinases in a cohort of 21 pairs of patient matched primary-brain metastases. **(B)** Ladder plot of RET expression changes. **(C)** RET 10X IHC staining of a representative sample from A. (Figure curtesy of Nolan Priedigkeit)

papillary thyroid cancer[96]. The facts that RET is increased only in breast cancer metastasis to brain, and GDNF is a brain specific growth factor, lead to the hypothesis that the overexpression of RET facilitates breast cancer brain metastasis due to the high levels of GDNF in the brain microenvironment.

The lab also recently completed whole exome sequencing on 12 pairs of patient matched primary and recurrent brain metastases (sample processing and sequencing done by Ryan Hartmaier PhD). Interestingly, we also identified a mutation in the kinase domain of RET (R969Q), that was highly enriched in the brain metastasis. ddPCR validation showed that the mutation was present in the primary tumor at an allele frequency of 0.45%, compared to 6.61% in the brain lesion, an increase of more than 14-fold (Figure 4B) (all mutation analysis and ddPCR validation done by Yijing Chen). A previous report also identified the RET mutation L851H, in a metastatic tumor, however no functional evaluation was done[97]. Aberrant activation of RET though translocations or point mutations has been shown to function as a driver of other cancer types; such as papillary thyroid cancer[96] and multiple endocrine neoplasia[98]. These alterations are believed to induce ligand independent receptor activity. If mutations in the kinase domain lead to GDNF independent RET signaling, it begs the question, why would the presence of GDNF in the brain microenvironment alter metastatic tropism? Given that we identified four other RET mutations in metastatic lesions in the MammaSeq cohort, and previous reports have identified RET mutations in non-brain metastatic lesions, it is possible that RET activation confers enhanced metastasis. This lead to the hypothesis that activating RET mutations enhances breast cancer metastasis, without specific metastatic tropism. Therefore, **I hypothesized that the overexpression of RET facilitates breast cancer brain metastasis, due to the high levels of GDNF in the brain microenvironment, while RET activating mutations enhance metastatic capacity without specific metastatic tropism.**

The most well-known function of RET is to promote the survival of neurons of both the central and peripheral nervous systems. However, mice deficient in any of GDNF, GFRA1, or RET, all have a similar phenotype, in which enteric neurons fail to migrate into the gastrointestinal

tract (among other complications), leading to death shortly after birth[99]. In BrCa cells, RET has been shown to promote resistance to endocrine therapies[100]. In pancreatic cancer cells, RET-GDNF signaling has been shown to promote the invasion of cells along the sciatic nerve[101]. Therefore, it is possible that active RET signaling in BrCa cells promotes survival and migration, leading to increased metastatic capacity. However, studies involving the effect of RET on BrCa metastasis are significantly lacking.

3.2 MATERIALS AND METHODS

3.2.1 Tissue Culture

All breast cancer cell lines used in this study were obtained from the American Tissue Culture Collection (ATCC). U251 glioblastoma cells that were used as a positive control for GDNF response, were a kind gift of Gary Kohanbash, John G. Rangos Sr. Research Center, Children's Hospital of Pittsburgh of UPMC, Pittsburgh PA. MCF-7 cells stably expressing ZS-Green were made by Susan Farabaugh, PhD (Adrian Lee Lab). Cultures were maintained as follows: MCF-7 and U251 cells were maintained in Dulbecco's Modified Eagle Medium (DMEM) supplemented with 10% fetal bovine serum (FBS) (Gibxo #26140-079), T47D in Roswell Park Memorial Institute (RPMI) 1640 Medium (Gibco #16600-082) supplemented with 10% FBS, and MDA-MB-134 (MM-134) in a 1:1 mixture of DMEM with Leibovitz-15 (Gibco #11415-064) media supplemented with 10% FBS. For organotypic co-culture assays, dissection media consisted of Phenol-Red free DMEM supplemented with 20% FBS and antibiotic-antimycotic (Gibco #15240062).

3.2.2 Immunoblots

Protein lysates were isolated using RIPA buffer (50 mM Tris, pH 7.4, 150 mM NaCl, 1 mM EDTA, 0.5% Nonidet P-40 (Sigma #21-3277), 0.5% NaDeoxycholate, 0.1% SDS), supplemented with Protease and Phosphatase Inhibitor (Thermo #78442), sonicated in a cup horn sonicator (for 5 minutes in 30 second pulses), and centrifuged for 15 minutes at 14,00 rpm at 4°C. All samples were quantified for protein concentration using BCA Assay (Pierce #23225) and 25-50μg (actual amount noted in figure legend) were run on an 8% SDS-PAGE gel. Protein was then transferred to a PVDF membrane (Millipore #IPFL00010) and incubated in Odyssey PBS Blocking buffer (LiCor #927-40000) for one hour and probed with antibodies. Primary antibodies used in this project are as follows: RET (Cell Signaling AB-3223), p-Tyr905-RET (Cell Signaling Ab-3221), p-Tyr1062-RET (Abcam ab51103), GFRα (Abcam Ab8026), p-Ser473-Akt (Cell Signaling Ab-4060), p-(Thr202/Tyr204)-MAPK (Cell Signaling Ab-4377), and β-actin (Sigma #A5441). All primary antibodies were probed overnight at 4°C. After removing primary, membranes were washed with TBST (50mM Tris, 150mM NaCl, 0.1% Tween 20, pH 7.4) three times, for 15 minutes each, and then incubated with secondary antibody at 1:20,000 at room temperature for 1hr. Secondary antibodies used were anti-mouse 800CW (LiCor#925-32210) and anti-rabbit 800CW (LiCor#925-32211). Membranes were again washed 3 times in TBST prior to imaging on Odyssey Infrared Imaging System (LiCor). For blots that were stripped and re-probed, 1X NewBlot Stripping buffer (LiCor #928-40032) was used per manufacturer's protocol.

3.2.3 Proliferation Assays

GDNF (Sigma-Aldrich #G1777) was suspended in water to a concentration of 1μg/μL, aliquoted, and stored at -80°C. MCF-7 and T47D cells were plated at 10,000 cells/well, MM-134 cells were plated at 20,000 cells/well, in 96-well 2D (Fisher #353072) or flat bottom ultra-low attachment

(ULA) (Corning #3473) plates. Cells were seeded in full serum media and allowed to adhere overnight. The next day, media was removed, the cells were washed twice with PBS, and cells were treated with cell line matched media supplemented 0.5% serum and GDNF at the marked concentration. Vehicle control wells were supplemented with water. Only the inner 60 wells (6x10) were used in experimental set up. Exterior wells were filled with an equal volume of PBS to prevent evaporation from the inner wells.

3.2.4 Scratch Assays

Matrigel (Corning #356234) was diluted in cell line specific, full serum media to a concentration of 100μg/mL. 50μL of matrigel solution was added to each well, and incubated at 37°C for 1hr before cells were seeded on top of the Matrigel. MCF-7, T47D, and U25 cells were plated at 150,000 cells/well, MM-134 cells were plated at 200,000 cells/well, in Essen ImageLock 96-well plates (Essen #4379). Cells were allowed to adhere overnight, before washing with PBS and creating the wound. Wounds were made with an Essen WoundMaker per the manufacture's protocol. Cells were then washed again with PBS and media supplemented with FBS and GDNF were added to each well. Wound healing was then monitored using IncuCyte Zoom software for 72hrs. At the end of each experiment, pictures from each well were manually curated to ensure that scratches were consistent, and results were not confounded by cells proliferating from within the wound. Outliers were manually removed.

3.2.5 Transwell Assays

The pDONR223-RET[102] donor vector (Addgene plasmid #23906), pLX302[103] destination vector (Addgene plasmid #25896), and BP Clonase II Reaction Mix (ThermoFisher Scientific #11789020) were used to generate a RET expression vector, where by expression was under the control of a cytomegalovirus (CMV) promoter and enhancer. One-Shot Stbl3 competent cells were

transformed via heat shock, according to the Addgene bacterial transformation protocol. E. Coli cells were grown on LB agar (Fisher BioReagents #9734) plates supplemented with 100μg/mL Ampicillin (VWR Life Science #VRWV0339) at 37°C overnight. The next day, colonies were picked from the plate and cultured in 5mL of LB media (Fisher BioReagents #9735) supplemented with 50 μg/mL Ampicillin, and cultured in a shaker at 37°C for approximately 8hrs. Media was then diluted into 500mL of LB media supplemented with Ampicillin, and cultured at 37°C overnight (~16hrs). Plasmid DNA was then isolated using a Plasmid Maxi Kit (Qiagen #12163).

BrCa cells were transfected using Lipofectamine 3000 (Invitrogen #L3000015), per manufacturers protocol. 24hrs after transfection, cells were tripsonized, pelleted, washed with PBS, suspended in media supplemented with 0.5% serum, and seeded into the upper chamber of 24-well 8.0μm (pore size) transparent PET membrane inserts (BD Falcon #353097) at 300,000 cells/well. The lower chambers of each well were filled with media supplemented with 0.5% serum, and 100ng/mL GDNF for experimental groups. Cells were cultured at 37°C for 72hrs, after which the upper side of each insert was cleaned with a cotton swab (Puritan #806-WC) and rinsed with ice-cold PBS. The inserts were then simultaneously fixed and stained with crystal violet (Sigma #C3886) in water plus 40% methanol for 20 minutes. The inserts were then washed with water and imaged. Finally, the staining intensity was measured using a Millipore colorimetric chemotaxis migration assay kit (Millipore #ECM508), according to the manufacture's protocol.

3.2.6 Organotypic Co-culture Assays

Organotypic co-culture protocol was a modified version of previously published reports.[104, 105] 4-week-old FBV/B6 mice were sacrificed by CO2 euthanasian. The brain and a kidney from each animal was quickly harvested, rinsed in ice-cold PBS, and transferred to ice-cold dissection media. The brains were then mounted to the vibratome stage using tissue adhesive (3M #1469SB) and

sectioned into 250μm thick slices. The slices were then transferred to 0.4μm polycarbonate membranes (Corning #3412) and cultured at 37°C overnight to allow cells to recover after the sectioning process. The next day, media was removed from the upper chamber of the membrane inserts. Roughly 100,000 MCF-7 cells (stably expressing ZS-Green) suspended in 10μL media were added directly on top of the slices. Inserts were incubated at 37°C for 20 minutes before fresh media was added back to the upper chamber of the inserts.

Fixation and staining protocol used was a modified version of previously published methods[106]. Briefly, slices were cultured at 37°C for 72hrs, washed with PBS, and then fixed in 4% PFA overnight at 4°C. Slices were then washed with PBST three times, and incubated in permeabilization buffer (PBST + 0.1% Triton X-100 – Fisher BioReagents #BP151) for 24hrs at room temperature. Slices were again washed with PBST (3X) and then incubated with blocking buffer (4% Bovine Serum Albumin – Sigma #A9647) for 2hrs at room temperature. Slices were then incubated in primary antibody (GFAP – Millipore #MAB360) diluted in blocking buffer at 1:400 at 4°C overnight, washed with PBST (3X), and incubated in secondary antibody (Alexa Fluor 546 Goat anti-Mouse – Life Technologies #A11018) at 4°C overnight. After washing, slices were mounted, upside down onto coverslips (Thermo - ProLong Diamond with Dapi #P36966), and left to dry overnight, at room temperature, in a dark sealed container.

3.2.7 Statistics

Technical replicates for all experiments are as described in figure legends. Heatmap in figure 6A was created in R, all other graphs and were made in GraphPad Prism. Dose responses were fitted with nonlinear four parameter functions to determine IC50 values. For transwell assays, significance was tested using a standard t-test. For growth curve assays, significance was tested

using one-way ANOVA test (Dunnett's multiple comparisons test). All statistical tests for this study were done in GraphPad Prism.

3.3 RESULTS

3.3.1 Identification of Cell Line Models

To identify cell line models for this project, we screened the cancer cell line encyclopedia[107](CCLE) for breast cancer cell lines that express both RET and the co-receptor GFRA1 (Protein: GFRα). Further examining the cell lines at the protein level, we identified 2 cell line models that express both RET and co-receptor: ER-positive ductal carcinoma MCF-7, and ER-positive lobular carcinoma cell lines MDA-MB-134 (MM-134). An immunoblot of a panel of cell lines from within the lab correlated well with the RNA expression and indicated cell lines with both high and low expression (Figure 6). T47D cells, which do not express RET, but which do express minimal levels of the co-receptor GFRα were used as a negative control for GDNF signaling experiments.

3.3.2 Breast Cancer Cells Have Functional GDNF-RET Signaling Pathway

Previous studies have shown that breast cancers cells that express RET, including MCF-7 cells, will activate Pi3K/AKT and MAPK/ERK pathways upon GDNF treatment, indicating a functional signaling mechanism[108, 109]. However, in my hands I did not find that GDNF treatment (100 ng/mL for 30min or 1hr) lead to a detectable enhancement of phosphorylation of the RET receptor at either Try-905 or at Try-1062 (Figure 17A & C). After 24hrs of serum starvation, GDNF treatment did not induce a noticeable change in AKT or MAPK phosphorylation (Figure 17B). This lack of consistency may be due to heterogeneity between strains of cell lines, or may be correctable with further experimental optimization. I also screened a panel of mutations, previously cloned by Yijing Chen, for RET and AKT activation (Figure 17). R969Q appeared to

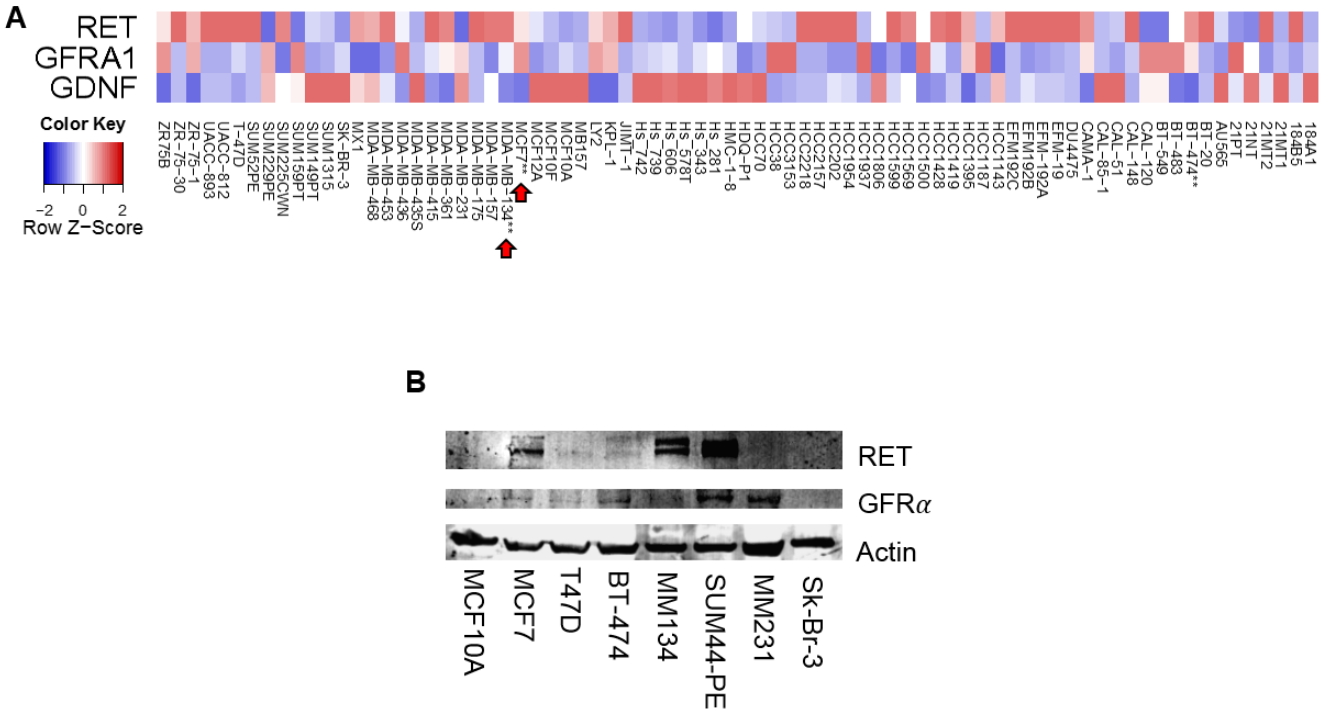

Figure 6: Identifying RET positive cell line models.
(A) Heatmap of expression data from CCLE. Arrows indicate cell lines used in subsequent studies. **(B)** Confirmation of RET and GFRαexpression in a panel of BrCa cell lines. 35µg lysate was loaded into each lane of the gel.

show RET activation in the absence of GDNF treatment, while L851H did not respond to GDNF treatment. However, the positive control, M918T (known to cause MEN2A[98]), did not show evidence of elevated phosphorylation independent of GDNF. Overexpression of the wild-type receptor, in the absence of GDNF, led to apparent receptor activation (Figure 17C). While I have not yet determined if these results are repeatable, meaning we cannot draw any significant conclusions from this experiment, it is possible that overexpression of the receptor leads to increased independent of GDNF. Previous reports have suggested that RET can form heterodimers with other RTKs, including the HER family receptors and MET. One possible mechanism of

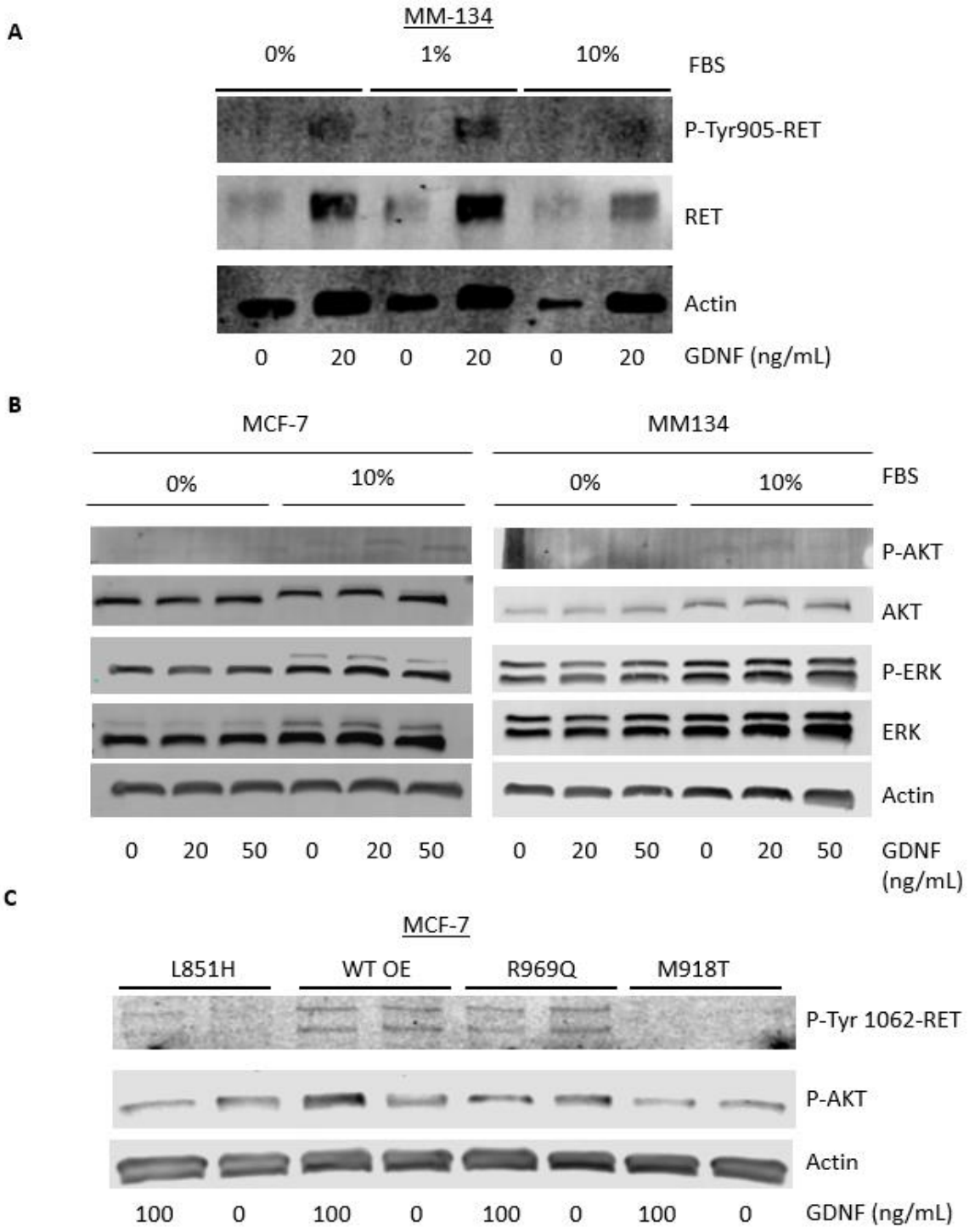

Figure 7: GDNF treatment of RET positive MCF-7 and MM-134 cell lines does not induce detectable increases in p-RET, p-AKT, or p-MAPK.
(A & B) Cells were cultured for 24hrs in the indicated serum concentration, and then stimulated with GDNF for 30 min. **(C)** MCF-7 cells were transfected with each indicated mutation (WT OE: wild-type overexpression), cultured overnight in media supplemented with 0.5% serum and stimulated with GDNF for 30 min.

GDNF independent RET activation is heterodimerization with another RTK that can induce transphosphorylation.

3.3.3 GDNF has a Limited Effect on 2D Growth, yet Significantly Enhances Anchorage Independent Growth of RET Positive IDC MCF-7 Cells

Given the classical function of RTKs to promote proliferation, I first sought to determine if GDNF-RET signaling in breast cancer cells enhanced growth. Despite the lack of pathway activation data, GDNF treatment promoted proliferation in 2D in both MCF-7 and MM-134 cells, after 7 days in culture (MCF-7 experiments repeated three independent times, MM-134 experiments repeated two independent times) (Figure 7A). Importantly, experiments were performed in 0.5% serum and there was no significant effect until after 3 days in culture. This suggests that effect of GDNF may not be noticeable until serum resources become depleted. In ultra-low attachment (ULA) plates GDNF treatment had a profound effect on growth of MCF-7 cells, but not MM-134(Figure 7B). For MCF-7 cells, this result repeated (twice) in both flat-bottom and round-bottom ULA plates. MM-134s are a lobular carcinoma derived cell line that are known to have complete loss of E-Cadherin expression[110], and known to grow well in the ULA environment[111].

3.3.4 GDNF Enhances Migration of MCF-7 Cells and acts as a Chemoattractant when Ret is Overexpressed

I next sought to determine if GDNF-RET signaling enhanced the migration of BrCa cells. Utilizing scratch assays, monitored with IncuCyte, I found that GDNF treatment increased cell migration in MCF-7 cells (effect seen in three independent experiments), but albeit in a limited and non-significant manner (all treatment groups compared to no treatment control at day 3 by one-way ANOVA $P > 0.07$) (Figure 8). MM-134 cells, did not migrates in this setting, as the no treatment control only closed 5% of the wound after 3 days. While this was highly consistent across n=6

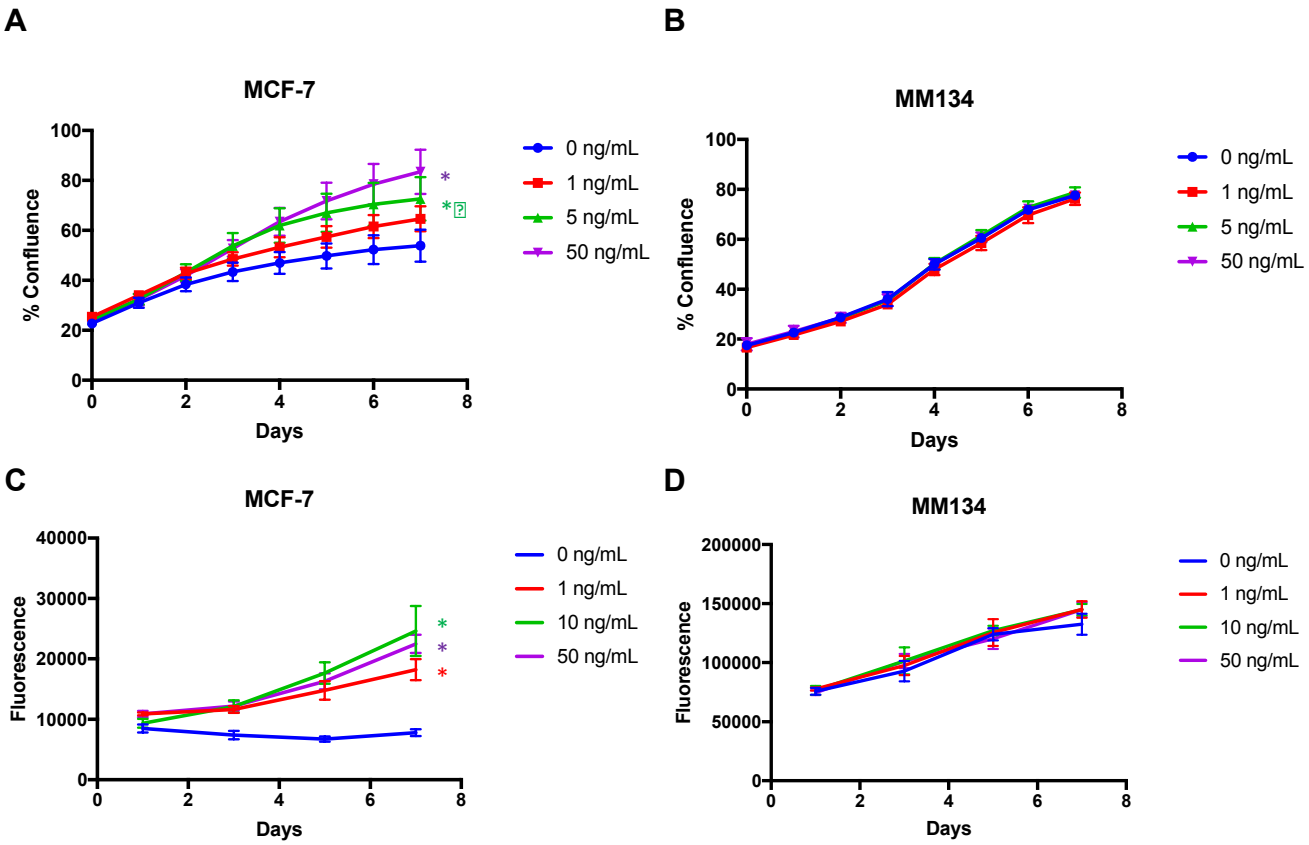

Figure 8: GDNF enhances growth of MCF-7 cells in 2D and ULA environments.
(A) 2D and **(C)** ULA growth curves of MCF-7 cells. **(B)** 2D and **(D)** ULA growth curves of MM-134 cells. 2D plates were monitored using IncuCyte Zoom software (n=6) and ULA plates were quantified using PrestoBlue cell viability assay (n=3). Bars represent mean ± SD. P<0.001 for each treatment compared to vehicle treated control at day 7 (one-way ANOVA).

replicates, the small effect size of GDNF limits the interpretation and functional significance of this result. Representative images of wound closure for MCF-7 and MM-134 cells are shown in Figures 19 and 20 respectively.

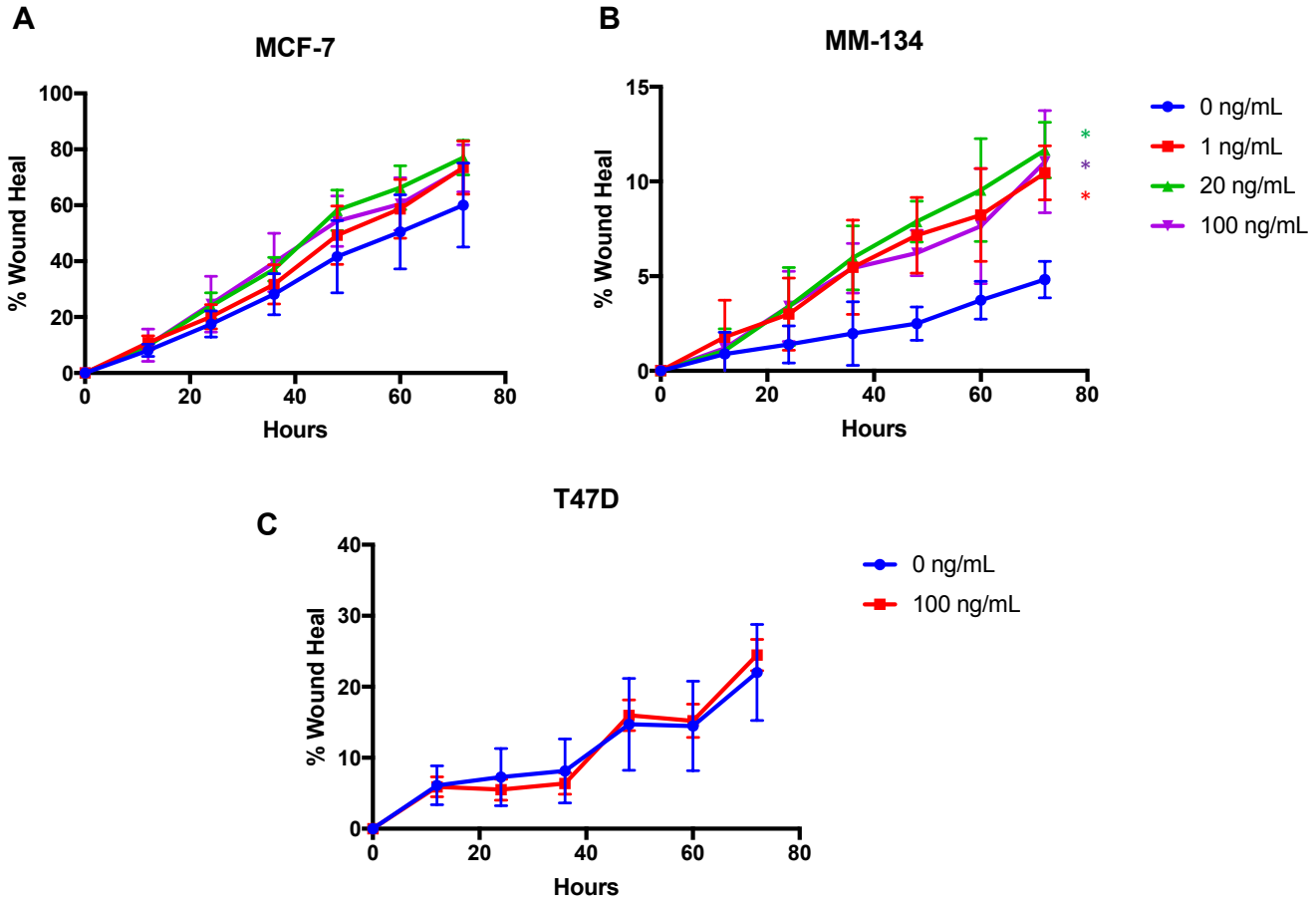

Figure 9:GDNF enhances migrationo of RET-positive MCF-7 and MM-134 cells, but not RET-negative T47D cells.
(A) MCF-7, **(B)** MM-134, and **(C)** T47D scratch assays monitored with IncuCyte zoom. Plots show the percentage of the original wound filled with invading cells at each time point. Points mark the mean ± SD of n=6 replicates. * $P < 0.005$.

Given that there are differences in proliferation rates upon GDNF treatment in MCF-7 cells (Figure 7), it is likely this effect reflects both proliferation than migration. In repeated proliferation assays with the MCF-7 and MM-134 cells, in the same experimental conditions, the effect on proliferation after 3 days is limited (From Figure 7 - at 3 days' growth, only 20ng/ml vs 0ng/mL was statistically significant, one-way ANOVA P=0.019). The lack of significance in proliferation after 72hrs, combined with the dose dependence of the effect seen in the scratch assays, suggests that GDNF treatment has a small effect on migration in MCF-7 cells.

To further explore the possibility that GDNF promotes metastasis through migration, I utilized transwell assays with GDNF as a chemoattractant. The U251 neuroblastoma cell line that has previously been shown to respond to GDNF treatment in transwell assays[112] was used as a positive control. Consistent with previously published results, MCF-7 cells did not have a strong migratory phenotype in this setting[111]. However, when RET was transiently overexpressed, increased staining in GDNF treated wells was apparent, compared to no treatment controls (Figure 9). This visual increase did not lead to a significant increase in crystal violet absorbance (t-test P= 0.258) in either of two independent repeats of the same experiment. Nonetheless, these results suggest that GDNF may act as a chemoattractant for cells highly expressing RET.

3.3.5 GDNF Does not Elicit a Significant Cytoprotective Effect After Serum Starvation or After DNA Intercalating Chemotherapy Treatment

After seeing that GDNF had a greater effect on proliferation, as serum resources became depleted, I next sought to determine if GDNF treatment has an effect on serum starvation induced apoptosis. Using either PrestoBlue, a measure of cellular metabolism, or Celltitre-Glo, a measure of total DNA content, GDNF treatment did not have a significant effect on cell survival after 7 days of serum starvation. The Celltitre-Glo readout indicates that after 7 days, total DNA levels were not dramatically reduced, indicating that serum starvation did not induce a significant level of apoptosis (Figure 21). Future experiments could utilize a live cell cleaved caspase-3 fluorescence dye to continuously monitor apoptosis over a longer duration.

As a more clinically relevant model to assess the cytoprotective effects of GDNF-RET signaling, I performed preliminary experiments utilizing the DNA intercalating chemotherapeutic agents Mitomycin-C and Doxorubicin to induce apoptosis (Figure 10). The IC50 values for the

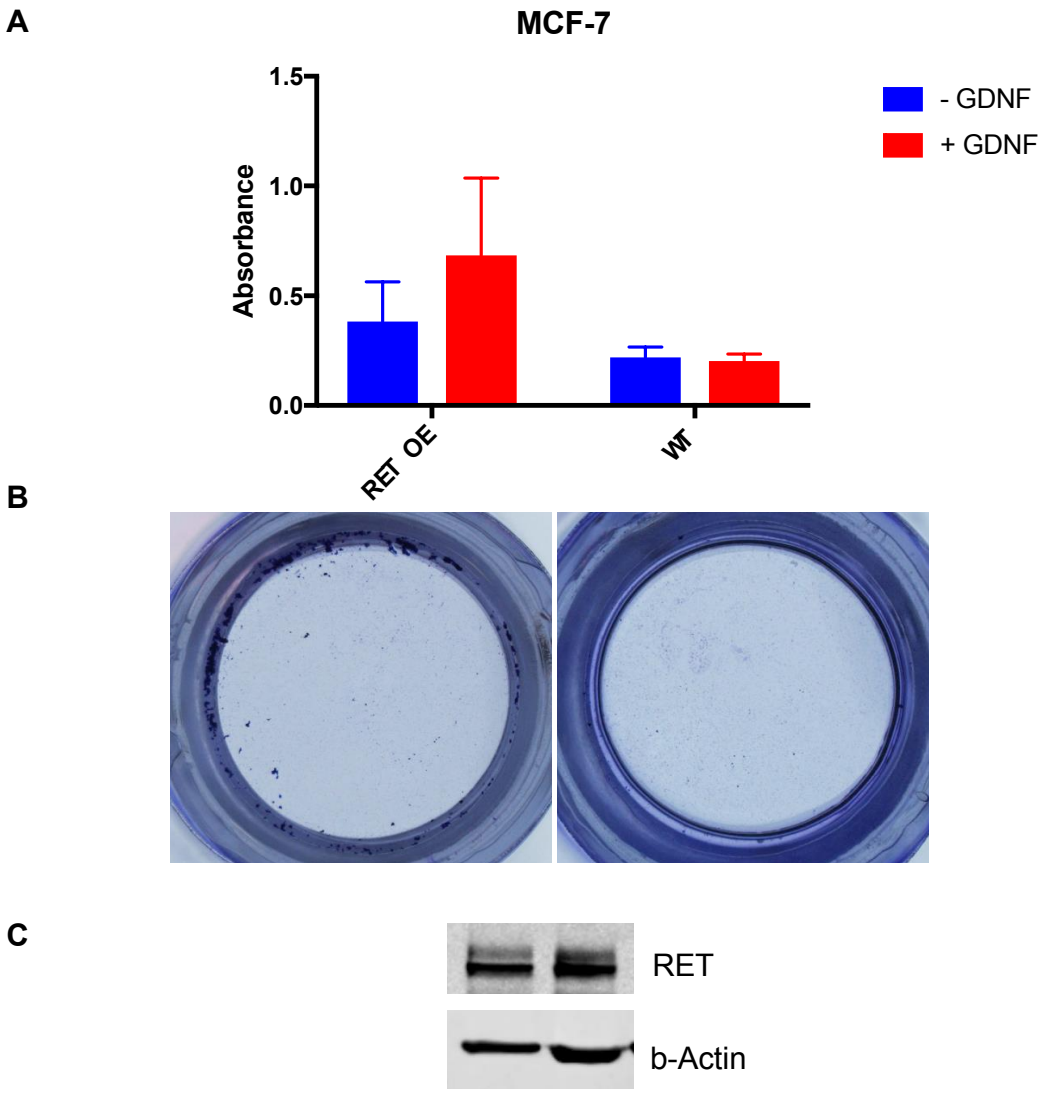

Figure 10: GDNF acts as a chemoattractant for MCF-7 cells transiently overexpressing RET in transwell assays.
(A) Quantification of transwell migration assays with MCF-7 cells migrating towards 100 ng/mL GDNF after transient overexpression of RET. Error bars indicate standard deviation of n=3 replicates. (**B)** Representative images of RET overexpression in wells with 100 ng/mL GDNF (Left) and with no chemoattractant (Right). (**C)** Western blot confirmation of transient RET overexpression.

treatment of MCF-7 cells with Mytomycin-C in the presence or absence of GDNF were 0.58 and 3.21μM respectively, and 2.26 and 0.40μM for T47D cells respectively. The IC50 values for Doxorubicin in the presence and absence of 100ng/mL GDNF were 37.6 and 23.3μM respectively

for MCF-7 cells, and 4.70 and 8.21μM for T47D cells respectively. At higher concentrations of drug, for both Mytomycin-C and Doxorubicin, the fluorescence ratio is lower in the presence of GDNF, however this an effect of low levels of proliferation induced by GDNF in the no treatment, normalization group.

It must be noted that these experiments were not repeated multiple times, therefore I cannot estimate the variance in IC50 values, and cannot determine if the differences in IC50 values are statistically significant. I speculate, based on the variance in the data and the similarity between the dose response curves, that these differences are not significant for either drug in T47D cells, or MCF-7 cells

3.3.6 Organotypic Co-Cultures, an in *Vitro* Method for Investigating Breast Cancer Cell Line Behavior in the Brain Microenvironment.

Recently, groups have reported organotypic co-culture systems, which mimic an in *vivo* microenvironment of a specific organ in *vitro*. Valiente *et al.* utilized this method to visualize how breast cancer cells (MDA-MB-231) invade along brain capillaries[105] and Askoxylakis *et al.* utilized a similar method to determine the efficacy of a novel trastuzamab drug conjugate for the treatment of HER2 positive cell line explants (BT474 and MDA-MB-361) in brain slices[104]. To determine how MCF-7 cells grow in this environment, we stably infected MCF-7 cells with Zsgreen (from Susan Farabaugh, PhD) and grew them on slices of brain tissue harvested from FVB/Black 6 mice. When 15,000 cells were added on top of the slices, after 3 days of culture no Zsgreen labelled cells could be visualized (data not shown). However, when 150,000 cells were

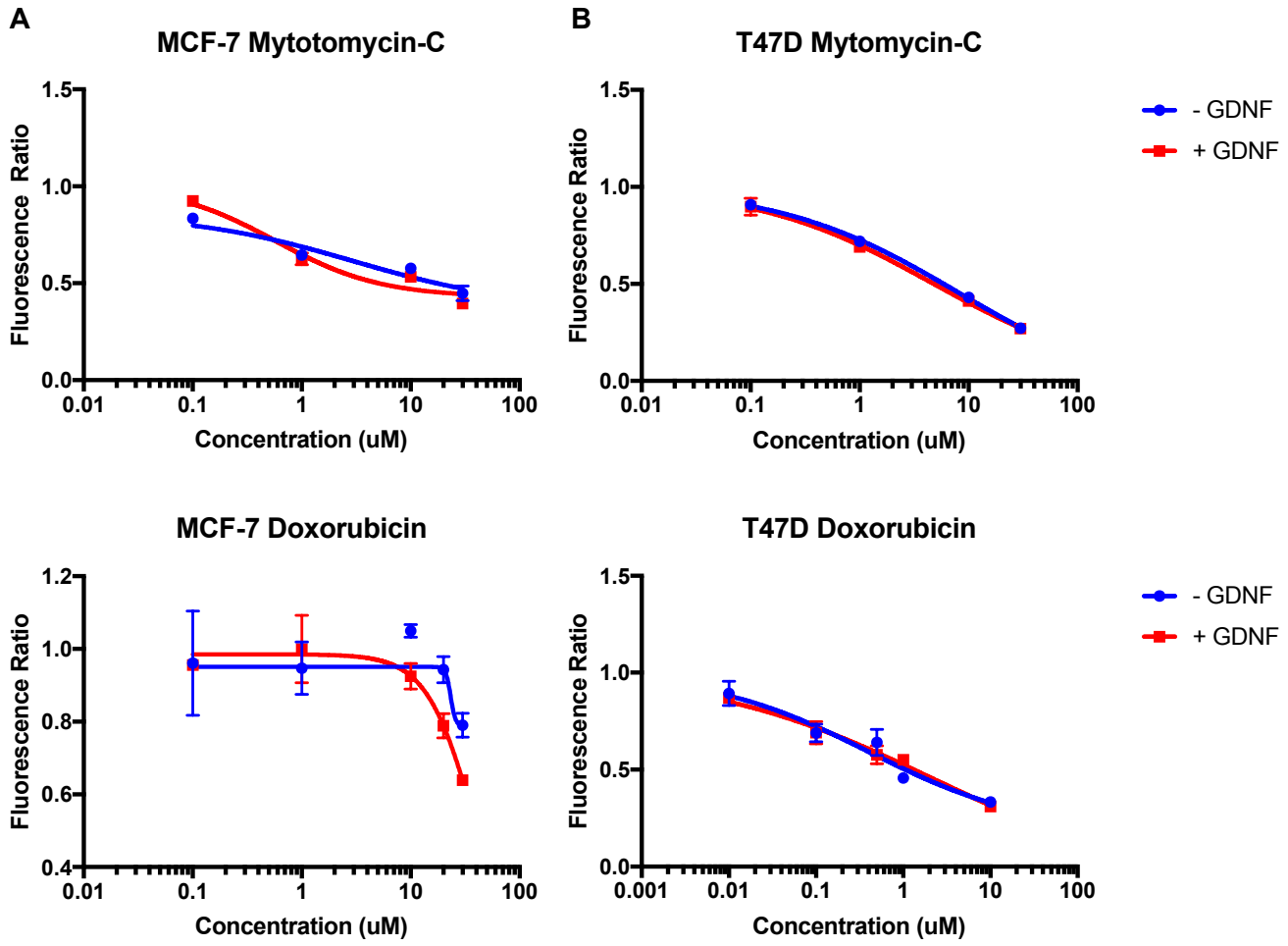

Figure 11: GDNF alters drug response to DNA intercalating agents Mytomycin-C and Doxorubicin in MCF-7 cells, but not T47D cells.
(A) MCF-7 and **(B)** T47D dose response curves of treatment with Mytomycin-C (TOP) or Doxorubicin (BOTTOM), in the presence or absence of 100ng/mL GDNF. All points (mean ± SD of n=3 replicates) were measured 3 days after treatment.

added on top of the slices, large clusters of labelled cells could be seen growing on the slices (Figure 11. D-F).

One of the challenges of working with thick sections of tissue, is that the staining protocol needs to be thoroughly optimized for the given experiment. We stained slices for both DAPI and GFAP, to visualize cell nuclei and GDNF releasing glial cells (mainly astrocytes), however for the vast majority of the slices, no staining was seen. Near the edges of the slices a small number of the characteristic star shaped astrocytes could be identified (Figure 11G). Seeing as GFAP is an

intracellular intermediate filament protein, and was only visible in a small number of cells, it is likely that the permeabilization step failed to effectively reach the center of the slices. Both standard fluorescence microscopy and con-focal microscopy failed to produce high resolution images of cells embedded inside the tissue slices.

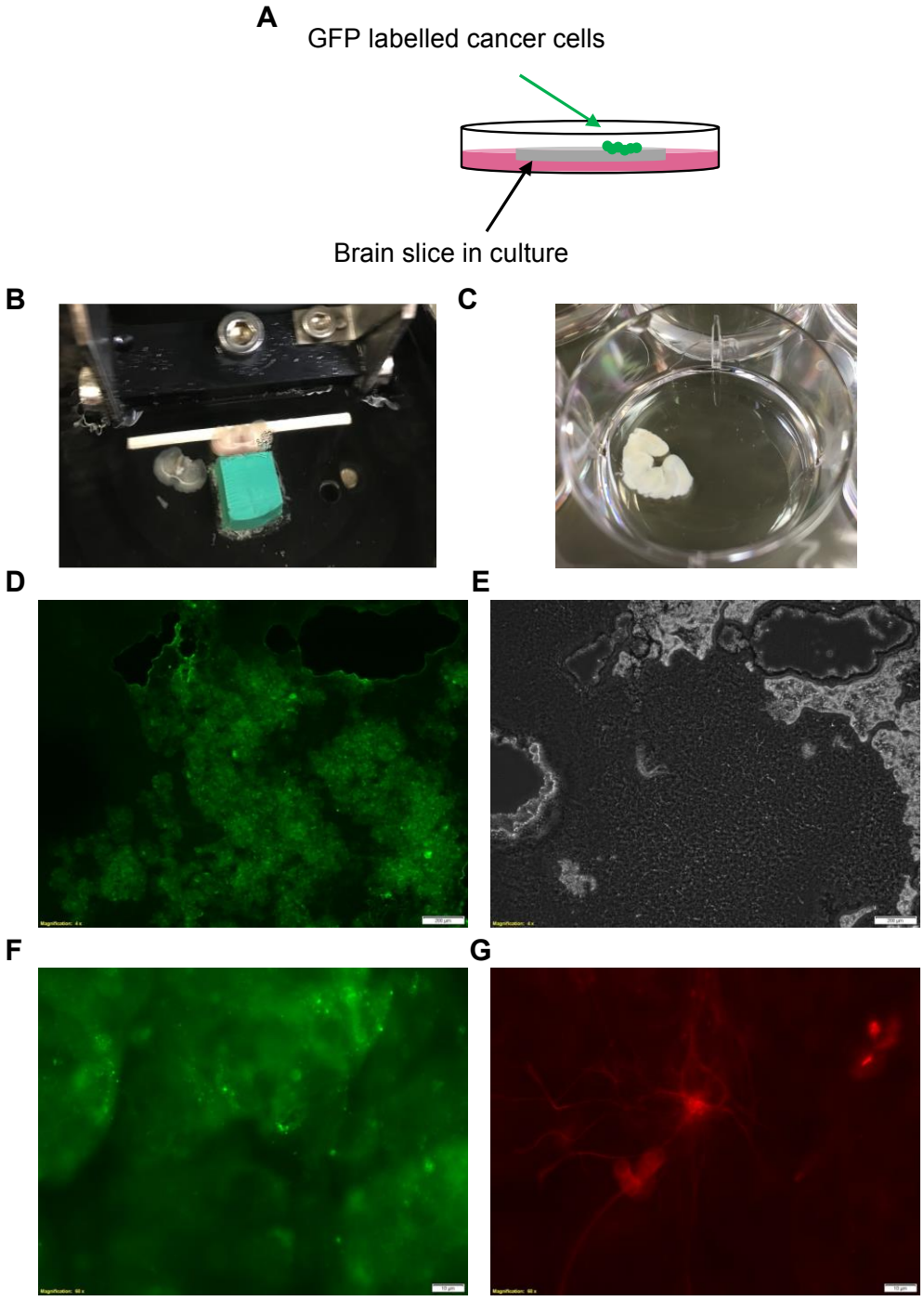

Figure 12: Organotypic co-culture assays with Zsgreen labelled MCF-7 cells.
(A) Schematic of assay set-up. Representative images of: **(B)** the sectioning process, **(C)** a 250um slice after fixation, co-localized **(D)** green fluorescence and **(E)** phase-contrast images of a macro-tumor taken at 4x, and 60x images of **(F)** Zsgreen labelled cells and **(G)** red fluorescence GFAP staining.

3.4 DISCUSSIONS

Understanding the genetic drivers of metastatic tropism is paramount to developing novel targeted therapies for therapy resistant metastatic cancers. Recent studies from our lab have implicated RET in breast cancer metastasis, with a particular focus on brain metastasis. A few studies have highlighted the importance of GDNF-RET signaling in breast cancer endocrine therapy resistance[30, 109, 113], and others have investigated it in the context of pancreatic cancer perineural invasion[101]. To our knowledge, this is the first study examining RET with a specific focus on breast cancer brain metastasis.

We were unable to confirm previous reports that in breast cancer cells, specifically MCF-7 cells, GDNF treatment induces RET, AKT, and MAPK phosphorylation. However, in functional growth and migration assays we see a clear functional effect of GDNF treatment. Most significant, is the effect of GDNF treatment on MCF-7 cell growth when plated in low density in ULA plates. The majority of the in *vitro* studies showed a clear trend, but not a significant effect. MCF-7 cells, while they do express RET, don't have DNA level amplifications or abnormally high levels of RET mRNA. When RET was overexpressed, we were able to induce a migration phenotype not previously seen with MCF-7 cells in our lab. While the expression level seen in our RNA-Seq brain cohort and published in the CCLE (with the caveat of different technology platforms) are comparable, it is possible that utilizing a cell line with higher RET expression would improve results. Future studies would include expanding assays to include MM-134 and SUM-44 cells, cell lines that highly express RET, or stably overexpressing RET in an IDC cell line such as MCF-7s or BT-474s.

Interestingly, after 3 days of treatment with a high dose of GDNF (100ng/mL) and a low dose of Mytomycin-C (0.1μM), there was a stark difference in cell number between GDNF treated

and untreated groups (relative to untreated groups). Mytomycin-C is known to induce apoptosis in a cleaved caspase-3 (CC3) dependent manner[114] and inhibition of the Pi3K/Akt pathway has been shown to promote apoptosis through the activation of CC3. Therefore, it is possible that at low doses of Mytomycin-C, RET mediated activation of PI3K shifts the signaling axis more towards pro-survival/proliferative phenotypes, inducing a noticeable increase in cell number. A similar effect was observed with Doxorubicin treatment, only at a higher concentration of 1μM.

While the organotypic co-culture assays failed to produce granular results, if there are vast differences after RET knockdown or RET overexpression, this method can be an effective way to visualize difference in tumor formation in the brain microenvironment. The main advantage of this assay, as opposed to standard co-culture or in *vitro* treatment methods, is that the brain slices incorporate all types of neuronal cells and mimic the environment in 3D. Future studies, would include monitoring growth of RET positive BrCa cell lines on these brain slices, and the efficacy of targeted RET therapies in this setting. While these studies provide a strong basis for investigating RET mutations and the role of RET in BrCa brain metastasis, further work is needed before strong conclusions can be draw.

4.0 DISCUSSIONS

The past decade has brought a targeted therapy revolution to cancer therapy. And while 5-year survival rates for primary disease continue to improve[38], breakthroughs in the treatment of metastatic disease have been few and far between. Understanding the biological mechanisms driving therapeutic resistance and metastatic tropism is an essential first step in identifying novel drug targets and developing new therapeutic strategies.

The rapid adoption of genetically stratified clinical trials for targeted therapies presents providers with a new challenge - offering patients a cost-effect approach to identify actionable mutations and match patients with targeted clinical trials. To help address this challenge, many groups have developed targeted mutation panels, that utilize massively parallel sequencing technologies[36, 37, 115, 116]. This allows oncologists to survey thousands of mutational hotspots in a single assay. Consistent with the UPMC study by Gurda *et al.*[63], a recent study by Pezo *et al.* published in 2017 found that relatively few (15%) metastatic breast cancer patients who undergo clinical sequencing enrolled in genotype-matched clinical trials, and as such there was virtually no survival benefit in undergoing the tests[59]. They suggested that more comprehensive sequencing efforts were needed. In chapter 2, we found that the limiting factor in matching patients with targeted therapies, was the lack of clinical evidence of mutation actionability. Despite finding nearly 600 protein coding mutations in carefully selected hotspot regions, only 26 mutations were considered clinically actionable by the OncoKB precision oncology database.

In this MammaSeq sequencing cohort, we identified 4 mutations in the kinase domain of RET. Interestingly, this gene also came up 2 recent studies done by previous members of the Lee Lab. RET was one of the most recurrently upregulated genes in a cohort of 21 patient-matched primary breast cancers and recurrent brain metastases. In a separate whole-exome sequencing

project, we found that another RET kinase domain mutation, R969Q, was enriched by more than 12-fold in a metastatic brain lesion, compared to the patient matched primary tumor. These studies suggest that this gene was being selected for in the brain microenvironment.

While we were not able to confirm that the mutation was activating, we did find that GDNF treatment of RET positive breast cancer cell lines alters cell growth and migration. Specifically, GDNF treatment elevated proliferation of MCF-7 cells over the course of 7 days of treatment in a low serum setting, significantly elevated anchorage independent growth of MCF-7 cells, and enhanced migration of MCF-7 and MM-134 cells in scratch assays. When RET was transiently overexpressed in MCF-7 cells, GNDF acted as a chemoattractant, inducing migration in a noticeable, yet insignificant level.

Taken together, these studies demonstrate the clinical feasibility of using MammaSeq to detect clinically actionable mutations in breast cancer patients, and provide provisional data supporting the investigation of RET signaling as a potentially targetable mediator of breast cancer brain metastasis.

APPENDIX A

SUPPLEMENTAL FIGURES

A1: TARGETED MUTATION DETECTION IN ADVANCED BREAST CANCER USING MAMMASEQ: SUPPLEMENTAL FIGURES

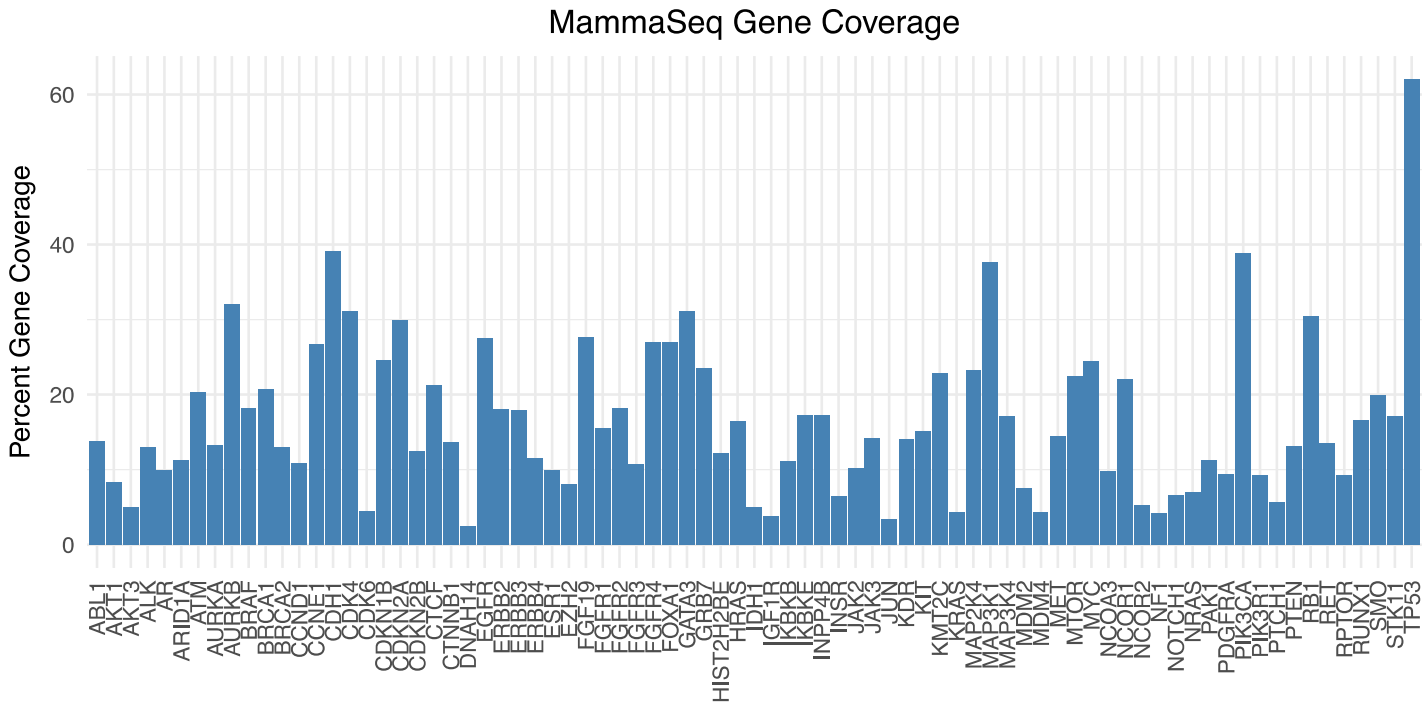

Figure 13: MammaSeq panel gene coverage.
Figure represents the percentage of protein coding base pairs in each gene covered by the MammaSeq panel.

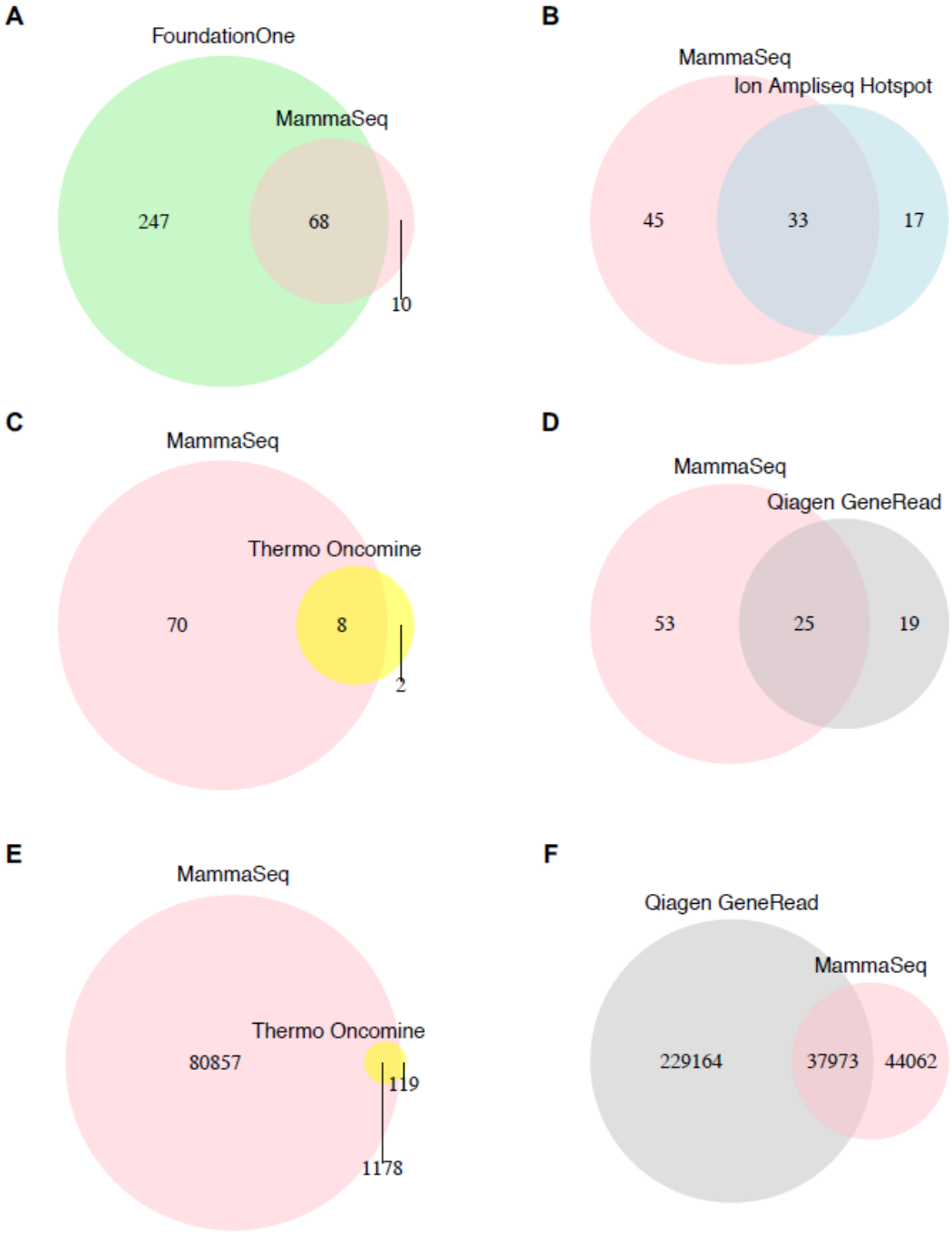

Figure 14: Coverage overlap between MammaSeq and select commercially available panels used in breast cancer.
Overlap of genes present in the MammaSeq panel and the **(A)** Foundation Medicine FoundationOne panel **(B)** Thermo Ion AmpliSeq Cancer Hotspot Panel (v2) **(C)** Qiagen GeneRead Human Breast Cancer Panel and the **(D)** Thermo Oncomine Breast cfDNA Assay. Overlap of the number of base pairs covered for the **(E)** Qiagen GeneRead and **(F)** Thermo Oncomine panels were calculated as these panel designs are publicly available.

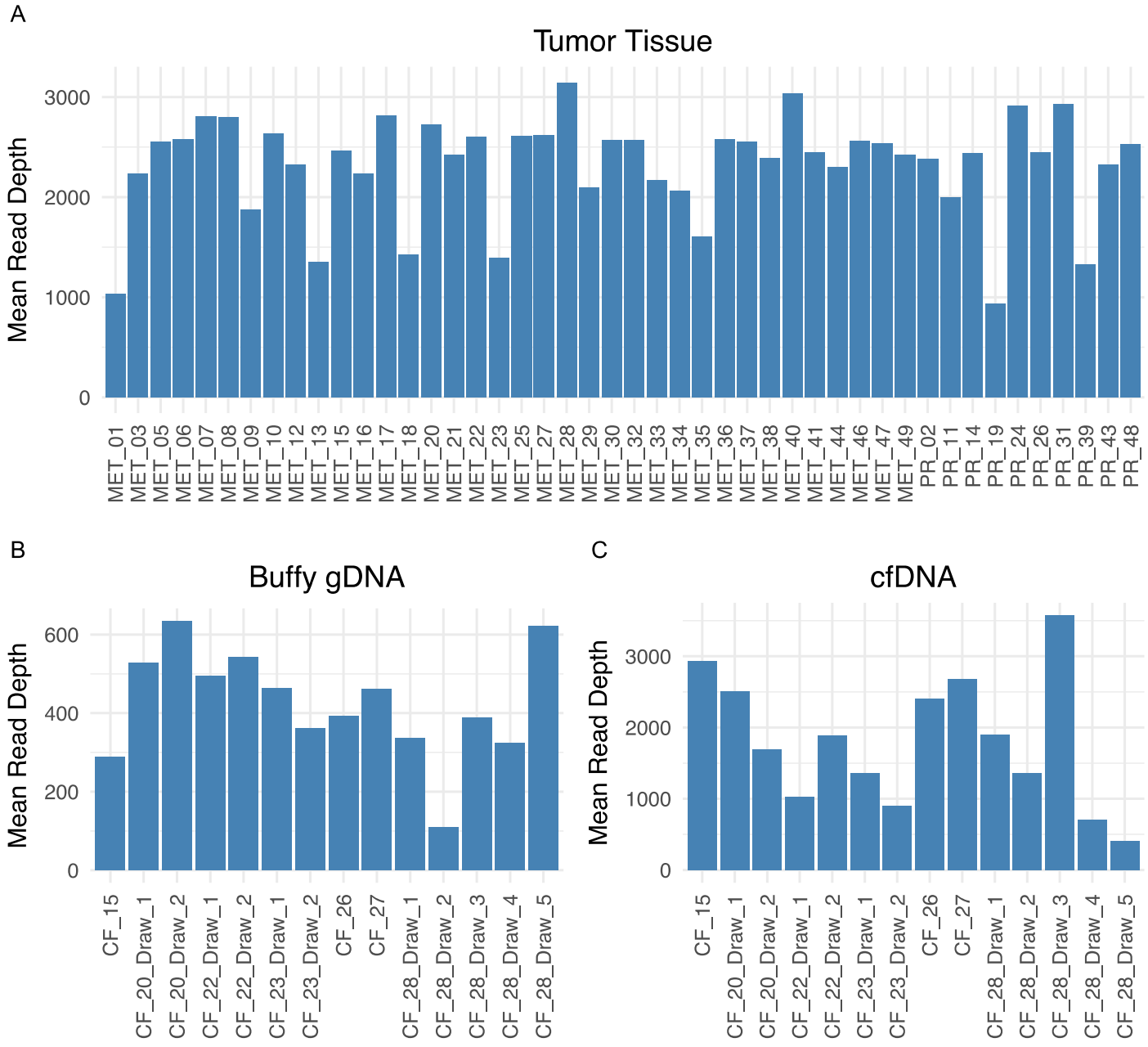

Figure 15: All samples were sequenced to sufficient to depth for accurate variant calling. Mean sequencing read depth for (A) the 46 solid tumor cohort, (B) isolated mononuclear cells from the 14 cfDNA blood draws, and (C) the 14 cfDNA samples.

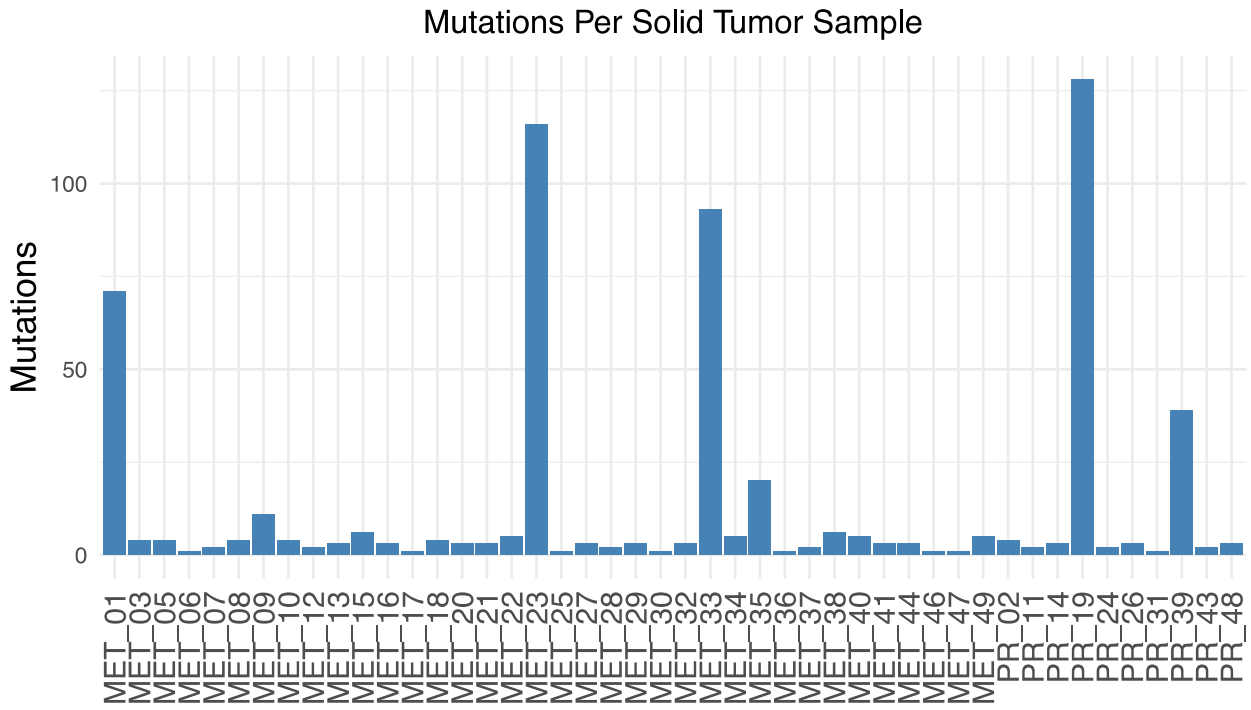

Figure 16: Tumor mutational Burden across all samples in the 46 solid tumor cohort.
Figure represents the total number of protein coding mutations for each sample.

A

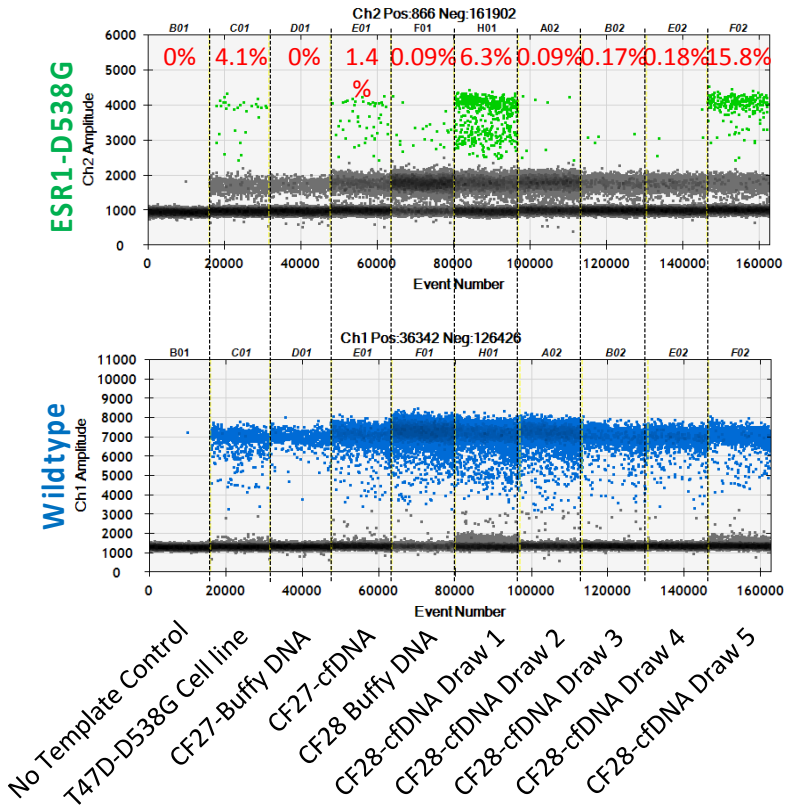
Ch2 Pos:866 Neg:161902
ESR1-D538G
Ch2 Amplitude
0%
4.1%
0%
1.4 %
0.09%
6.3%
0.09%
0.17%
0.18%
15.8%
Event Number
Ch1 Pos:36342 Neg:126426
Wildtype
Ch1 Amplitude
Event Number
No Template Control
T47D-D538G Cell line
CF27-Buffy DNA
CF27-cfDNA
CF28 Buffy DNA
CF28-cfDNA Draw 1
CF28-cfDNA Draw 2
CF28-cfDNA Draw 3
CF28-cfDNA Draw 4
CF28-cfDNA Draw 5

B

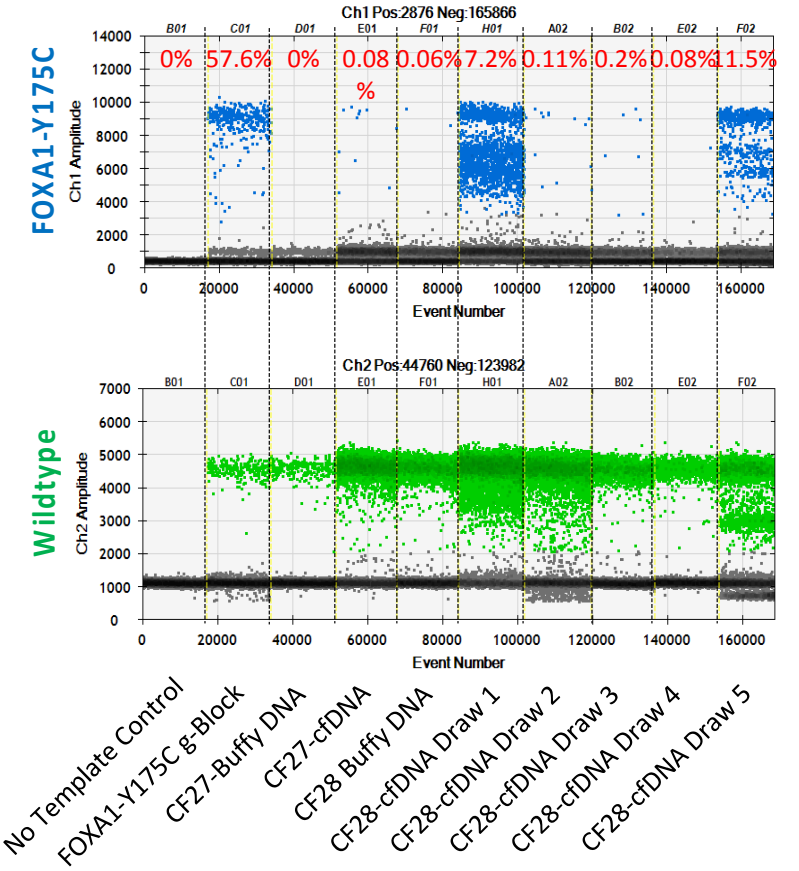
Ch1 Pos:2876 Neg:165866
FOXA1-Y175C
Ch1 Amplitude
0%
57.6%
0%
0.08 %
0.06%
7.2%
0.11%
0.2%
0.08%
11.5%
Event Number
Ch2 Pos:44760 Neg:123982
Wildtype
Ch2 Amplitude
Event Number
No Template Control
FOXA1-Y175C g-Block
CF27-Buffy DNA
CF27-cfDNA
CF28 Buffy DNA
CF28-cfDNA Draw 1
CF28-cfDNA Draw 2
CF28-cfDNA Draw 3
CF28-cfDNA Draw 4
CF28-cfDNA Draw 5

C

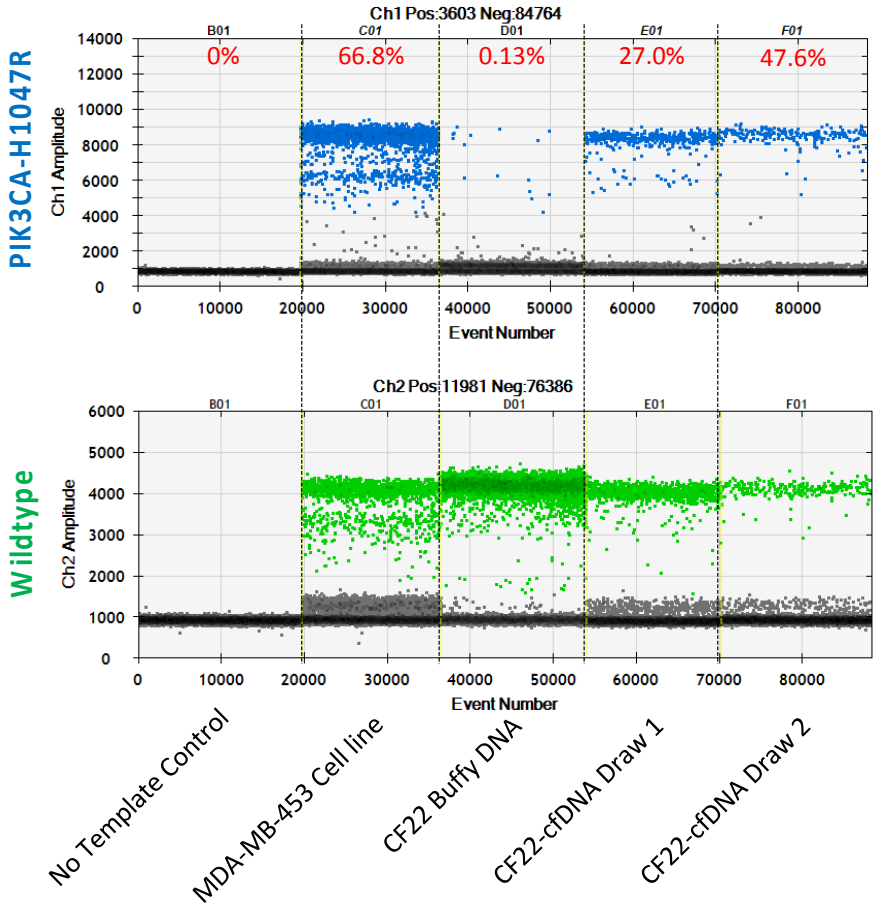

Figure 17: ddPCR validation of mutations identified by MammaSeq.
Figures represent the fluorescence intensity of each droplet (colored points represent droplets positive for the indicated fluorophore and grey points represent negative droplets) and calculated mutation allele frequencies for **(A)** ESR1-D538G, **(B)** FOXA1-Y175C, and **(C)** PIK3CA-H1047R. (ddPCR done by Rekha Gyanchandani PhD)

A2: INVESTIGATING THE ROLE OF RET IN BREAST CANCER METASTASIS

MCF-7

100 ng/mL GDNF

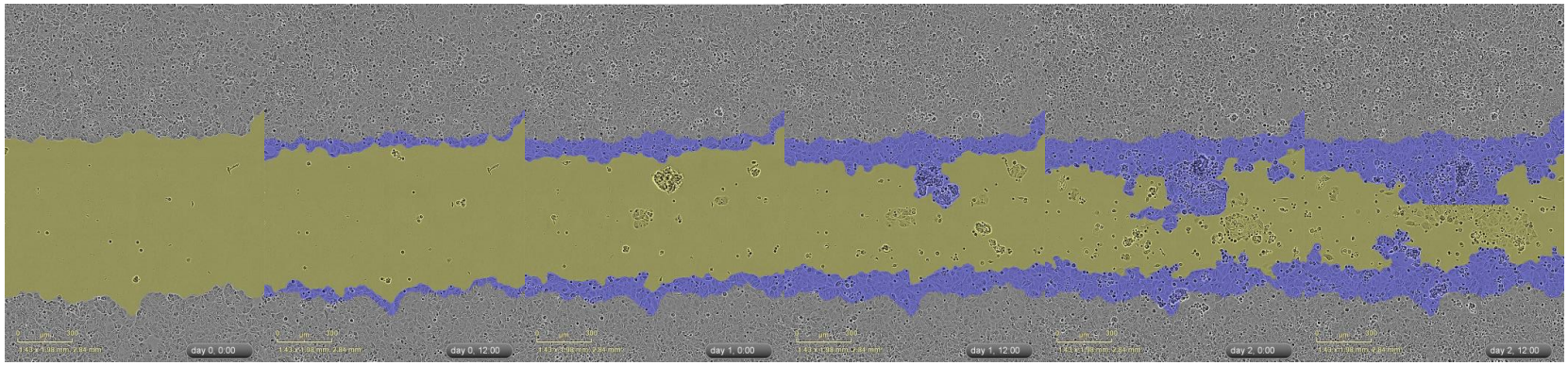

0 ng/mL GDNF

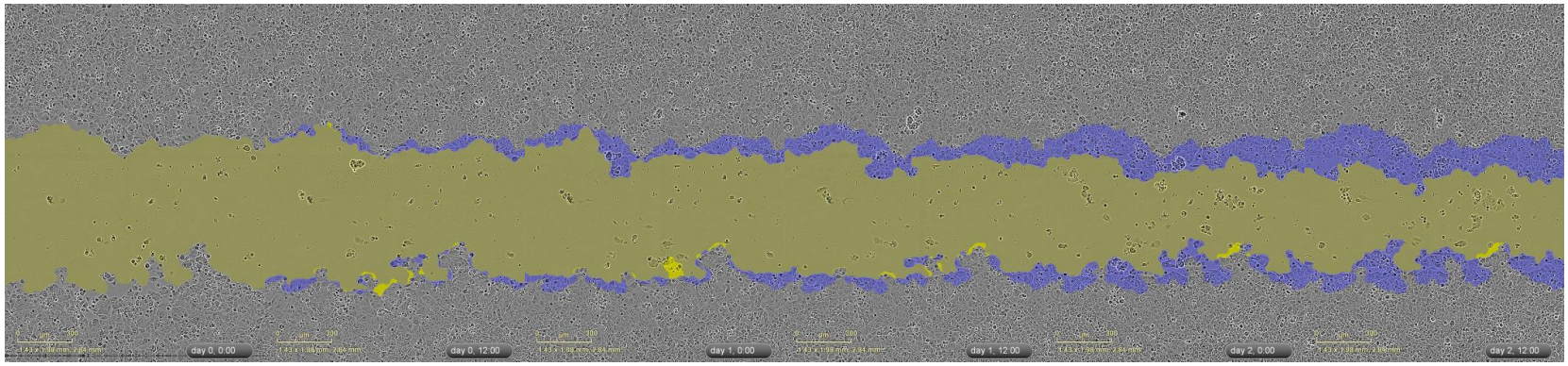

Figure 18: GDNF enhances migration of MCF-7 cells in scratch assays.
IncuCyte images taken every 12hrs after scratches were made. Yellow shading represents the width of the original scratch and purple shading shows the area of invasion by the cells. Quantification of images shown in figure 8.

100 ng/mL GDNF

MM-134

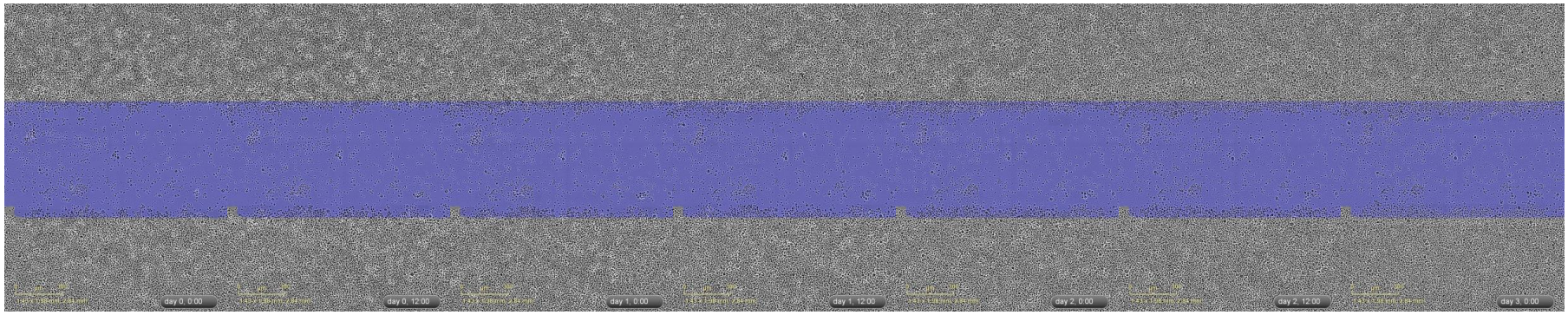

0 ng/mL GDNF

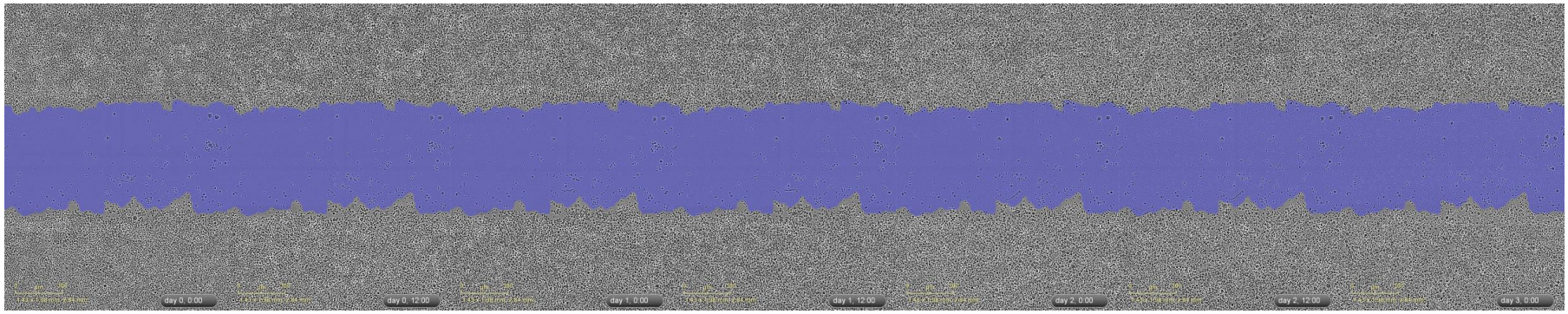

Figure 19: GDNF enhances migration of MM-134 cells in scratch assays.
IncuCyte images taken every 12hrs after scratches were made. Quantification of images shown in figure 8.

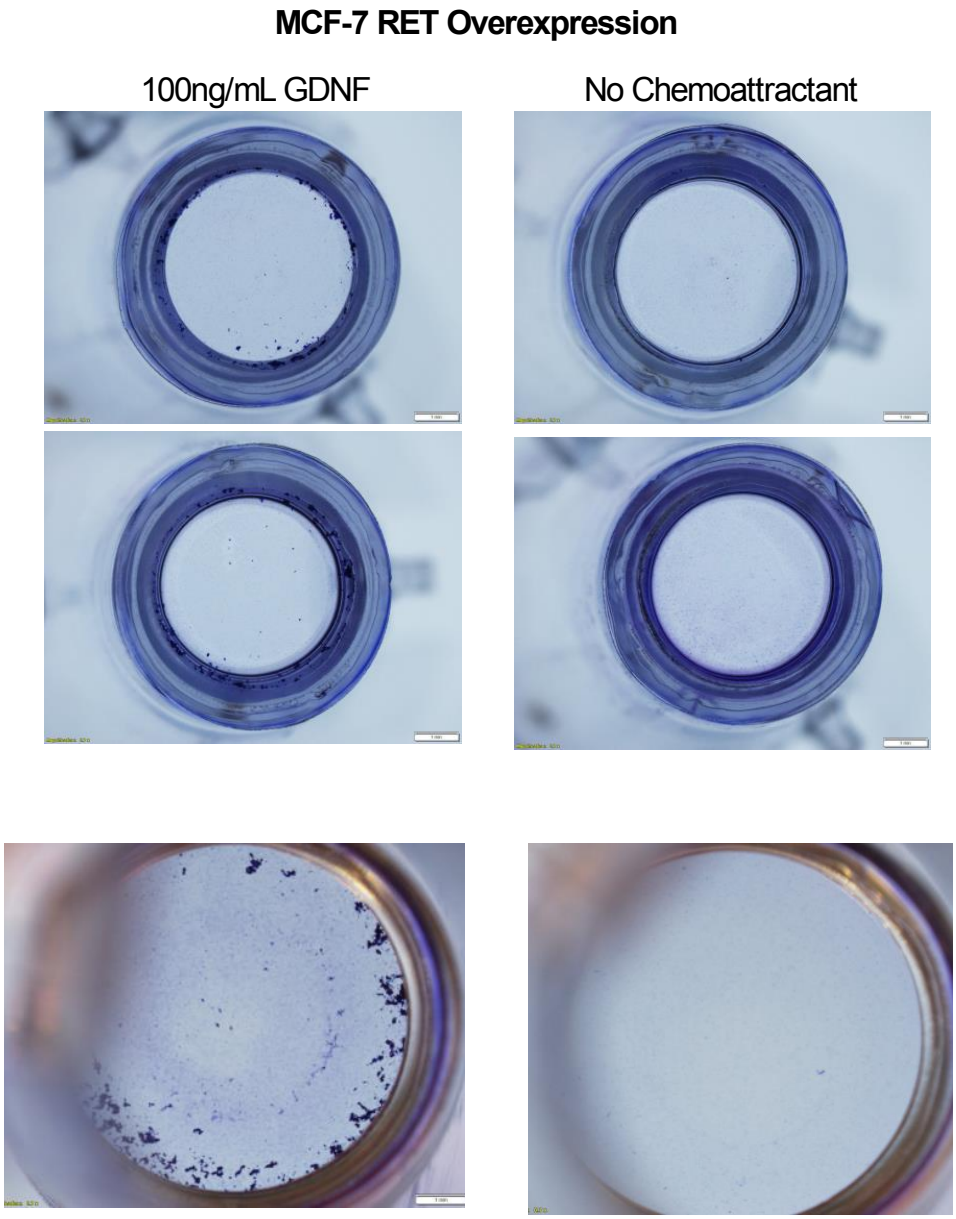

Figure 20: GDNF acts as a chemoattractant for MCF-7 cells transiently overexpressing RET. Figures show representative images from two independent repeats of the same experiment.

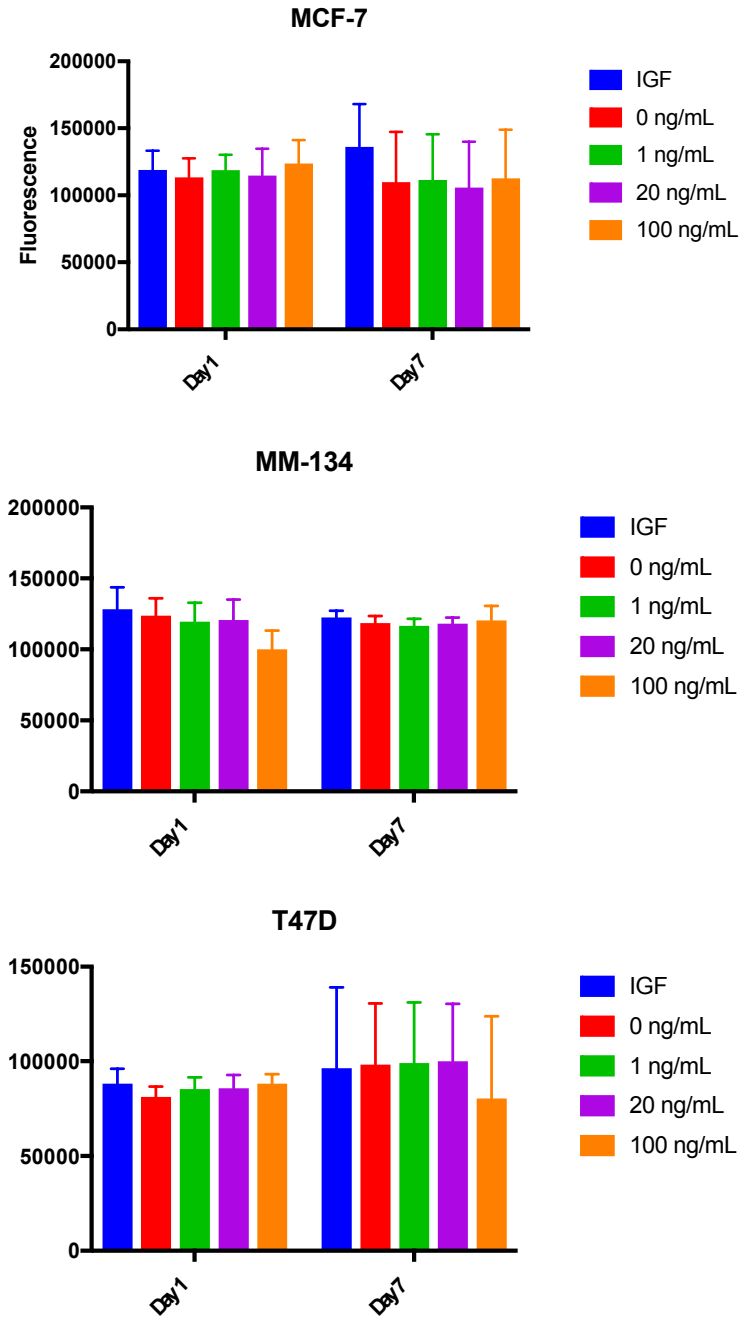

Figure 21: GDNF does not have a significant effect on cell number after 7 days of serum starvation.
40,000 cells per well were plated in full serum containing media, allowed to adhere overnight, and treated with GDNF containing serum-free media. Day 0 marks the beginning of treatment. Figures show CellTitre-Glo quantification of cells at day 1 and day 7 after treatment. Plots show mean ± SD of n=12 replicates.

APPENDIX B

SUPPLEMENTAL TABLES

Table 4: Clinical characteristics, treatment, and outcome data for all patients in MammaSeq cohorts.

Patient ID for manuscript	Age at Diagnosis	Race 1-Desc	Histo/Behavior ICD-O-3-Desc	Grade/Differentiation	Size of Tumor	Clinical T	Clinical N	Clinical M	Clinical Stage Group	Pathologic T	Pathologic N	Pathologic M	Pathologic Stage Group	ER	PR	HER2	Vital Status-Desc	Disease-Free Survival	Months from Dx to 1st Recur	Survival
PR02	43	White	IDC	3	N/A	N/A	N/A	N/A	N/A	N/A	N/A	N/A	N/A	-	-	-	N/A	N/A	N/A	N/A
PR11	42	Black	IDC/ILC	3	72	c3	c0	c0	2B	p1C	p0	N/A	1A	-	-	-	Dead	15	17	22
PR14	41	White	IDC	3	17	c1C	c0	c0	1A	p1C	p1	N/A	2A	+	+	-	Dead	19	19	46
PR19	49	White	IDC	N/A	N/A	N/A	N/A	N/A	N/A	N/A	N/A	N/A	N/A	-	-	-	Dead	0	0	0
PR24	51	White	IDC	3	70	c2	c1	c0	2B	p4	p3A	N/A	3C	+	+	+	Dead	0	0	47
PR26	54	White	IDC	N/A	N/A	N/A	N/A	N/A	N/A	N/A	N/A	N/A	N/A	+	+	-	Dead	0	0	0
PR31	54	White	IDC	3	42	c2	c1	c0	2A	p1B	p1A	N/A	2A	+	+	-	Dead	15	15	37
PR39	64	White	IDC	2	60	c1C	c1	c0	2A	p3	p2A	N/A	3A	+	+	+	Alive	3	5	54
PR43	65	White	IDC	2	31	c2	c0	c0	2B	p2	p2A	N/A	3A	+	+	-	Dead	12	14	36
PR48	70	White	IDC	3	N/A	N/A	N/A	N/A	N/A	p4A	p2A	c0	3B	+	+	-	Dead	7	7	47
MET01	30	White	IDC	3	046	c2	c1	c0	2B	p2	p3A	N/A	3C	-	-	-	Dead	16	16	26
MET03	39	White	N/A	4	N/A	c4D	c0	c0	3B	pIS	p0	c0	0	-	-	+	Alive	92	92	127
MET05	32	White	IDC	3	065	c3	c3	c0	3C	p3	p3	N/A	3C	-	-	-	Dead	8	8	40
MET06	31	White	IDC	3	38	c2	c1A	c0	2B	p1B	p1A	c0	1	+	-	-	Dead	13	13	66
MET07	36	White	IDC	3	33	c2	c0	c1	4	p1C	p1A	p1	4	+	-	-	Dead	0	0	55
MET08	36	White	IDC	2	31	c2	c0		2A	p2	p2A		3A	+	+	-	Dead	32	33	61
MET09	38	White	IDC	3	80	c3	c1	c0	3A	pIS	p0		0	-	-	-	Dead	15	15	20
MET10	37	White	IDC	9	10	c1	c1	c0	2A	p1	p1		2A	+	-	-	Dead	52	52	67
MET12	42	White	IDC	3	20	c1C	c1	c0	2B	p1B	p0		1A	-	-	-	Dead	12	13	42
MET13	42	White	IDC	3	61	c3	c1	c0	3A	p2	p2A		3A	-	-	-	Dead	20	21	29
MET15	-	White	N/A	9	999								N/A	-	-	-	Dead	0	0	0
MET16	37	White	ILC	2	100	c3	c1	c0	3A	p1	p2A		3A	+	-	-	Dead	82	84	138
MET17	-	White	IDC	9	999								N/A	N/A	N/A	N/A	Alive	0	0	0
MET18	45	White	IDC	3	120	c3	c2	c1	4	p3	p1A	p1	4	-	-	-	Dead	0	0	25
MET20	47	White	ILC	3	58	c3	c1	c1	4	pX	pX		N/A	+	+	-	Dead	0	0	25
MET21	35	White	IDC	3	13	c1	c0	c0	1	p1C	p0	c0	1	+	+	+	Alive	32	33	221
MET22	36	White	N/A	9	13	cX	cX	c0	99	p1C	p0		1	-	-	-	Dead	84	84	181
MET23	47	White	Mix	3	35	c2	c1	c0	2B	p1B	p0		1A	-	-	-	Dead	25	25	63
MET25	42	White	Mix	2	50	c1	c0	c0	1	p2	p1	c0	2B	+	+	-	Dead	123	125	163
MET27	49	White	Mix	3	90	c3	c1	c0	3A	p2	p3	c0	3C	+	+	-	Dead	28	28	68
MET28	38	White	IDC	9	14	c1	c0	c0	1	p1C	pX	c0	N/A	+	+	+	Dead	63	64	213
MET29	54	White	IDC	3	999	c4B	c1		3B	pX	pX		N/A	-	-	-	Dead	0	0	18
MET30	45	White	IDC	9	60	c3	c1	c0	3A	p1C	p1	c0	2A	+	+	-	Dead	87	88	146
MET32	54	White	IDC	3	34	c2	c1	c1	4	p2	p0	p1	4	+	+	-	Alive	0	0	68
MET33	31	White	IDC	9	999	c1	c0	c0	1	p1	p0		1	+	-	+	Dead	274	274	348
MET34	45	White	IDC	2	030	c2	c1	c0	2B	p2	p0	c0	2A	N/A	N/A	N/A	Dead	42	43	201
MET35	48	White	ILC	9	120	c4B	c1	c0	3B	p3	p1	c0	3A	+	+	-	Dead	135	136	170
MET36	58	White	IDC	3	23	c2	c0	c0	2A	pX	pX		N/A	-	-	-	Dead	15	16	41
MET37	60	White	IDC	9	30	c2	cX	c1	4	p2	p3A	p1	4	-	+	-	Dead	0	0	26
MET38	45	White	ILC	9	42	c2	c0	c0	2A	p2	p1B	c0	2B	+	-	-	Dead	198	198	226
MET40	57	White	IDC	2	28	cX	cX	cX	99	p2	p1A	c0	2B	-	-	-	Dead	86	86	93
MET41	67	White	ILC	9	2	c1A	c0	c1	4	pX	pX		N/A	+	N/A	N/A	Alive	0	0	34
MET44	-	White	N/A	9	999								N/A	-	-	-	Dead	0	0	0
MET46	68	White	IDC	2	18	c1C	c0	c0	1A	p1C	p0		1A	+	-	-	Alive	4	6	40
MET47	69	White	IDC	3	12	cX	c0	c0	99	p1C	p0		1A	-	-	-	Alive	19	19	22
MET49	71	White	IDC	3	19	c2	c0	c0	2A	p1C	p0		1A	+	+	-	Dead	44	44	51
CF15	24	white	IDC	2	997	3	1	0	3A	1A	1	0	2A	+	+	N/A	1	79	79	138
CF20	53	white	IDC	3	074	3	1	0	3A	2	1A	0	2B	+	+	N/A	1	64	64	96
CF22	34	white	IDC	2	025	N/A	N/A	N/A	99	N/A	N/A	N/A	99	+	+	N/A	1	0	0	0
CF23	54	white	IDC	3	034	2	1	1	4	2	0	1	4	+	N/A	N/A	1	0	0	40
CF26	62	white	IDC	9	013	1C	3	0	3B	X	X	X	99	+	N/A	N/A	1	151	152	224
CF27	42	white	IDC	3	074	3	3	1	4	1C	3	1	4	+	+	N/A	0	0	0	80
CF28	55	white	IDC	2	018	1C	0	0	1	1C	1M	0	2A	+	+	N/A	1	116	117	124

Table 5: Sequence of primers for preamplification

Mutation	Forward primer	Reverse primer
ESR1-D538G	GCATGAAGTGCAAGAACGTG	AAGTGGCTTTGGTCCGTCT
FOXA1-Y175C	TGGATGGCCATGGTGATGAG	AGACGTTCAAGCGCAGCTA

Table 6: Sequence of ddPCR primers and probes

Mutation	Forward primer	Reverse primer	Mutant Probe	WT probe	Fluorescence
ESR1-D538G	GCATGAAGTGCAAGAACGTG	AAGTGGCTTTGGTCCGTCT	TCTATGGCCTGCTGCTGGAGATGCT	TCTATGACCTGCTGCTGGAGATGCT	HEX/FAM
FOXA1-Y175C	TGGATGGCCATGGTGATGAG	AGACGTTCAAGCGCAGCTA	CTACTCGTGCATCTCG	CCTACTCGTACATCTCG	FAM/VIC

REFERENCES

1. Siegel, R.L., K.D. Miller, and A. Jemal, *Cancer statistics, 2018.* CA Cancer J Clin, 2018. **68**(1): p. 7-30.
2. Siegel, R.L., K.D. Miller, and A. Jemal, *Cancer statistics, 2016.* CA Cancer J Clin, 2016. **66**(1): p. 7-30.
3. Beaston, G.T., B.A. Cantab, and M.D. Edinburgh, *On the Treatment of Inoperable Cases of Carcinoma of the Mamma: Suggestions for a New Method of Treatment, with Illustrative Cases.* Trans Med Chir Soc Edinb, 1896. **15**: p. 153-179.
4. Philips, J. and R.R. Love, *Oophorectomy for Breast Cancer: History Revisited.* Journal of the National Cancer Institute, 2002. **94**(19): p. 1433-1434.
5. Jensen, E.V., et al., *Estrogen Receptor and Breast Cancer Response to Adrenalectomy.* Natl Cancer Inst Monogr., 1971. **34**: p. 55-70.
6. Jordan, V.C., *Tamoxifen: a most unlikely pioneering medicine.* Nat Rev Drug Discov, 2003. **2**(3): p. 205-13.
7. King, C.R., M.H. Kraus, and S.A. Aaronson, *Amplification of a novel v-erbB-related gene in human mammary carcinoma.* Science, 1985. **229(4147):974-6**.
8. Ross, J.S., et al., *The HER-2 receptor and breast cancer: ten years of targeted anti-HER-2 therapy and personalized medicine.* Oncologist, 2009. **14**(4): p. 320-68.
9. Slamon, D., et al., *Adjuvant trastuzumab in HER2-positive breast cancer.* N Engl J Med, 2011. **365**(14): p. 1273-83.
10. Blows, F.M., et al., *Subtyping of breast cancer by immunohistochemistry to investigate a relationship between subtype and short and long term survival: a collaborative analysis of data for 10,159 cases from 12 studies.* PLoS Med, 2010. **7**(5): p. e1000279.
11. Makki, J., *Diversity of Breast Carcinoma: Histological Subtypes and Clinical Relevance.* Clin Med Insights Pathol, 2015. **8**: p. 23-31.
12. Morrogh, M., et al., *Cadherin-catenin complex dissociation in lobular neoplasia of the breast.* Breast Cancer Res Treat, 2012. **132**(2): p. 641-52.
13. Vallejos, C.S., et al., *Breast cancer classification according to immunohistochemistry markers: subtypes and association with clinicopathologic variables in a peruvian hospital database.* Clin Breast Cancer, 2010. **10**(4): p. 294-300.
14. Cheang, M.C., et al., *Ki67 index, HER2 status, and prognosis of patients with luminal B breast cancer.* J Natl Cancer Inst, 2009. **101**(10): p. 736-50.
15. Perou, C.M., et al., *Molecular Portraits of Human Breast Tumors.* Nature, 2000. **406**: p. 747-752.
16. Sorlie, T., et al., *Gene expression patterns of breast carcinomas distinguish tumor subclasses with clinical implications.* Proc Natl Acad Sci U S A, 2001. **98**(19): p. 10869-74.
17. Parker, J.S., et al., *Supervised risk predictor of breast cancer based on intrinsic subtypes.* J Clin Oncol, 2009. **27**(8): p. 1160-7.
18. *History of breast cancer therapy*. Medical Therapy of breast Cancer, ed. Z. Rayter. 2003, Bristol, UK: Cambridge University Press.
19. Wallden, B., et al., *Development and verification of the PAM50-based Prosigna breast cancer gene signature assay.* BMC Med Genomics, 2015. **8**: p. 54.
20. Sparano, J.A., et al., *Adjuvant Chemotherapy Guided by a 21-Gene Expression Assay in Breast Cancer.* N Engl J Med, 2018.
21. Cardoso, F., et al., *70-Gene Signature as an Aid to Treatment Decisions in Early-Stage Breast Cancer.* N Engl J Med, 2016. **375**(8): p. 717-29.

22. Burstein, H.J., et al., *Adjuvant endocrine therapy for women with hormone receptor-positive breast cancer: american society of clinical oncology clinical practice guideline focused update.* J Clin Oncol, 2014. **32**(21): p. 2255-69.
23. Cole, J.T., J. Lu, and A. Tremont, *Endocrine Therapy for Early Breast Cancer: Updated Review.* Ochsner Hournal, 2017. **17**(4): p. 404-411.
24. Giordano, S.H., et al., *Systemic therapy for patients with advanced human epidermal growth factor receptor 2-positive breast cancer: American Society of Clinical Oncology clinical practice guideline.* J Clin Oncol, 2014. **32**(19): p. 2078-99.
25. Hassan, *Chemotherapy for breast cancer (Review).* Oncology Reports, 2010. **24**(5).
26. Reinert, T., et al., *Clinical Implications of ESR1 Mutations in Hormone Receptor-Positive Advanced Breast Cancer.* Frontiers in Oncology, 2017. **7**(26).
27. Jeselsohn, R., et al., *ESR1 mutations-a mechanism for acquired endocrine resistance in breast cancer.* Nat Rev Clin Oncol, 2015. **12**(10): p. 573-83.
28. Turner, N., et al., *FGFR1 amplification drives endocrine therapy resistance and is a therapeutic target in breast cancer.* Cancer Res, 2010. **70**(5): p. 2085-94.
29. Oh, A.S., et al., *Hyperactivation of MAPK Induces Loss of ERa Expression in Breast Cancer Cells.* Molecular Endocrinology, 2001. **15**(8): p. 1344-1359.
30. Morandi, A., et al., *GDNF-RET signaling in ER-positive breast cancers is a key determinant of response and resistance to aromatase inhibitors.* Cancer Res, 2013. **73**(12): p. 3783-95.
31. Wada, R., S. Yagihashi, and Z. Naito, *mRNA expression of delta-HER2 and its clinicopathological correlation in HER2-overexpressing breast cancer.* Mol Med Rep, 2016. **14**(6): p. 5104-5110.
32. Hanker, A.B., et al., *An Acquired HER2(T798I) Gatekeeper Mutation Induces Resistance to Neratinib in a Patient with HER2 Mutant-Driven Breast Cancer.* Cancer Discov, 2017. **7**(6): p. 575-585.
33. Ciriello, G., et al., *Emerging landscape of oncogenic signatures across human cancers.* Nat Genet, 2013. **45**(10): p. 1127-33.
34. Curtis, C., et al., *The genomic and transcriptomic architecture of 2,000 breast tumours reveals novel subgroups.* Nature, 2012. **486**(7403): p. 346-52.
35. Cancer Genome Atlas, N., *Comprehensive molecular portraits of human breast tumours.* Nature, 2012. **490**(7418): p. 61-70.
36. Zehir, A., et al., *Mutational landscape of metastatic cancer revealed from prospective clinical sequencing of 10,000 patients.* Nat Med, 2017. **23**(6): p. 703-713.
37. Frampton, G.M., et al., *Development and validation of a clinical cancer genomic profiling test based on massively parallel DNA sequencing.* Nat Biotechnol, 2013. **31**(11): p. 1023-31.
38. Steeg, P.S., *Targeting metastasis.* Nat Rev Cancer, 2016. **16**(4): p. 201-18.
39. Weigelt, B., J.L. Peterse, and L.J. van 't Veer, *Breast cancer metastasis: markers and models.* Nat Rev Cancer, 2005. **5**(8): p. 591-602.
40. Nguyen, D.X. and J. Massague, *Genetic determinants of cancer metastasis.* Nat Rev Genet, 2007. **8**(5): p. 341-52.
41. Gupta, G.P. and J. Massague, *Cancer metastasis: building a framework.* Cell, 2006. **127**(4): p. 679-95.
42. Massague, J. and A.C. Obenauf, *Metastatic colonization by circulating tumour cells.* Nature, 2016. **529**(7586): p. 298-306.
43. Wang, M., et al., *Role of tumor microenvironment in tumorigenesis.* J Cancer, 2017. **8**(5): p. 761-773.
44. Paget, S., *The distribution of secondary growths in cancer of the breast.* Cancer Metastasis Rev., 1889. **2**: p. 98-101.

45. Langley, R.R. and I.J. Fidler, *The seed and soil hypothesis revisited--the role of tumor-stroma interactions in metastasis to different organs.* Int J Cancer, 2011. **128**(11): p. 2527-35.
46. Navarro-Olvera, J.L., et al., *Brain metastases: Literature review.* Revista Médica del Hospital General de México, 2017. **80**(1): p. 60-66.
47. Bos, P.D., et al., *Genes that mediate breast cancer metastasis to the brain.* Nature, 2009. **459**(7249): p. 1005-9.
48. Lee, B., et al., *Involvement of the Chemokine Receptor CXCR4 and Its Ligand Stromal Cell-Derived Facto 1a in Breast Cancer Cell Migration Through Human Brain Microvascular Endothelial Cells.* Mol Cancer Res, 2004. **2**(6): p. 327-338.
49. Wilkman, H., et al., *Relevance of PTEN loss in brain metastasis fromation in breast cancer patients.* Breast Cancer Res, 2012. **14**.
50. Saunus, J.M., et al., *Integrated genomic and transcriptomic analysis of human brain metastases identifies alterations of potential clinical significance.* J Pathol, 2015. **237**(3): p. 363-78.
51. DP., K. and F.G. Askoxylakis V, Sheng Q, Badeaux M, Goel S, Qi X, Shankaraiah R, Cao ZA, Ramjiawan RR, Bezwada D, Patel B, Song Y, Costa C, Naxerova K, Wong CSF, Kloepper J, Das R, Tam A, Tanboon J, Duda DG, Miller CR, Siegel MB6, Anders CK, Sanders M, Estrada MV, Schlegel R, Arteaga CL, Brachtel E, Huang A, Fukumura D, Engelman JA, Jain RK., *The brain microenviroment mediates resistance in luminal reast cancer to PI3K inhibition through HER3 activation.* Sci Transl Med, 2017.
52. Da Silva, L., et al., *HER3 and downstream pathways are involved in colonization of brain metastases from breast cancer.* Breast Cancer Research, 2010.
53. Brastianos, P.K., et al., *Genomic Characterization of Brain Metastases Reveals Branched Evolution and Potential Therapeutic Targets.* Cancer Discov, 2015. **5**(11): p. 1164-1177.
54. Nicholas G. Smith, et al., *Targeted mutation detection in advanced breast cancer using MammaSeq.* bioRxiv, 2018.
55. Harbeck, N., C. Thomssen, and M. Gnant, *St. Gallen 2013: brief preliminary summary of the consensus discussion.* Breast Care (Basel), 2013. **8**(2): p. 102-9.
56. Koren, S. and M. Bentires-Alj, *Breast Tumor Heterogeneity: Source of Fitness, Hurdle for Therapy.* Mol Cell, 2015. **60**(4): p. 537-46.
57. Hyman, D.M., B.S. Taylor, and J. Baselga, *Implementing Genome-Driven Oncology.* Cell, 2017. **168**(4): p. 584-599.
58. Kamps, R., et al., *Next-Generation Sequencing in Oncology: Genetic Diagnosis, Risk Prediction and Cancer Classification.* Int J Mol Sci, 2017. **18**(2).
59. Pezo, R.C., et al., *Impact of multi-gene mutational profiling on clinical trial outcomes in metastatic breast cancer.* Breast Cancer Res Treat, 2017.
60. Boland, M.G., et al., *Clinical next generation sequencing to identify actionable aberrations in phase I program.* Oncotarget, 2015. **6**(24).
61. Grzegorz T. Gurda, T.A., Marina N. Nikiforova, Yuri E. Nikiforov, Peter C. Lucas, David J. Dabbs, Adrian V. Lee, Adam M. Brufsky, Shannon L. Puhalla, Rohit Bhargava, *Characterizing Molecular Variants and Clinical Utilization of Next-generation Sequencing in Advanced Breast Cancer.* Appl Immunohistochem Mol Morphol, 2016. **00**(00).
62. Bose, R., et al., *Activating HER2 mutations in HER2 gene amplification negative breast cancer.* Cancer Discov, 2013. **3**(2): p. 224-37.
63. Gurda, G.T., et al., *Characterizing Molecular Variants and Clinical Utilization of Next-generation Sequencing in Advanced Breast Cancer.* Appl Immunohistochem Mol Morphol, 2016. **00**(00).
64. Wang, P., et al., *Sensitive Detection of Mono- and Polyclonal ESR1 Mutations in Primary Tumors, Metastatic Lesions, and Cell-Free DNA of Breast Cancer Patients.* Clin Cancer Res, 2016. **22**(5): p. 1130-7.

65. Lek, M., et al., *Analysis of protein-coding genetic variation in 60,706 humans.* Nature, 2016. **536**(7616): p. 285-91.
66. Genomes Project, C., et al., *A global reference for human genetic variation.* Nature, 2015. **526**(7571): p. 68-74.
67. Gu, Z., R. Eils, and M. Schlesner, *Complex heatmaps reveal patterns and correlations in multidimensional genomic data.* Bioinformatics, 2016. **32**(18): p. 2847-2849.
68. Talevich, E., et al., *CNVkit: Genome-Wide Copy Number Detection and Visualization from Targeted DNA Sequencing.* PLoS Comput Biol, 2016. **12**(4): p. e1004873.
69. Toy, W., et al., *ESR1 ligand-binding domain mutations in hormone-resistant breast cancer.* Nat Genet, 2013. **45**(12): p. 1439-45.
70. Robinson, D.R., et al., *Activating ESR1 mutations in hormone-resistant metastatic breast cancer.* Nat Genet, 2013. **45**(12): p. 1446-51.
71. Craig, D.W., et al., *Genome and transcriptome sequencing in prospective metastatic triple-negative breast cancer uncovers therapeutic vulnerabilities.* Mol Cancer Ther, 2013. **12**(1): p. 104-16.
72. Michael Ashburner, C.A.B., Judith A. Blake, David Botstein, Heather Butler1, J. Michael Cherry, Allan P. Davis, Kara Dolinski, Selina S. Dwight, Janan T. Eppig, Midori A. Harris, David P. Hill4, Laurie Issel-Tarver, Andrew Kasarskis, Suzanna Lewis, John C. Matese, Joel E. Richardson, Martin Ringwald, Gerald M. Rubin & Gavin Sherlock, *Gene Ontology: toll for the unification of biology.* Nature Genetics, 2000. **25**.
73. Wagner, A.H., et al., *DGIdb 2.0: mining clinically relevant drug-gene interactions.* Nucleic Acids Res, 2016. **44**(D1): p. D1036-44.
74. Bilgin, B., et al., *A current and comprehensive review of cyclin-dependent kinase inhibitors for the treatment of metastatic breast cancer.* Curr Med Res Opin, 2017. **33**(9): p. 1559-1569.
75. Turnbull, C., et al., *Genome-wide association study identifies five new breast cancer susceptibility loci.* Nat Genet, 2010. **42**(6): p. 504-7.
76. Chakravarty, D., et al., *OncoKB: A Precision Oncology Knowledge Base.* JCO | Precision Oncology, 2017.
77. Carter, H., et al., *Cancer-specific high-throughput annotation of somatic mutations: computational prediction of driver missense mutations.* Cancer Res, 2009. **69**(16): p. 6660-7.
78. Moline, J. and C. Eng, *Multiple endocrine neoplasia type 2: an overview.* Genet Med, 2011. **13**(9): p. 755-64.
79. Mulligan, L.M., *RET revisited: expanding the oncogenic portfolio.* Nat Rev Cancer, 2014. **14**(3): p. 173-86.
80. Bamford, S., et al., *The COSMIC (Catalogue of Somatic Mutations in Cancer) database and website.* Br J Cancer, 2004. **91**(2): p. 355-8.
81. Nik-Zainal, S., et al., *Landscape of somatic mutations in 560 breast cancer whole-genome sequences.* Nature, 2016. **534**(7605): p. 47-54.
82. Nishino, M., et al., *Monitoring immune-checkpoint blockade: response evaluation and biomarker development.* Nat Rev Clin Oncol, 2017. **14**(11): p. 655-668.
83. Clark, M., et al., *Effects of chemotherapy and hormonal therapy for early breast cancer on recurrence and 15-year survival: an overview of the randomised trials.* Lancet, 2005. **365**: p. 1687-1717.
84. Chalmers, Z.R., et al., *Analysis of 100,000 human cancer genomes reveals the landscape of tumor mutational burden.* Genome Med, 2017. **9**(1): p. 34.
85. Dawson, S.J., et al., *Analysis of circulating tumor DNA to monitor metastatic breast cancer.* N Engl J Med, 2013. **368**(13): p. 1199-209.
86. Bettegowda, C., et al., *Detection of circulating tumor DNA in early- and late-stage human malignancies.* Sci Transl Med, 2014. **6**(224): p. 224ra24.

87. Rothe, F., et al., *Plasma circulating tumor DNA as an alternative to metastatic biopsies for mutational analysis in breast cancer.* Ann Oncol, 2014. **25**(10): p. 1959-65.
88. Garcia-Murillas, I., et al., *Mutation tracking in circulating tumor DNA predicts relapse in early breast cancer.* Sci Transl Med, 2015. **7**(302): p. 302ra133.
89. Gyanchandani, R., et al., *Detection of ESR1 mutations in circulating cell-free DNA from patients with metastatic breast cancer treated with palbociclib and letrozole.* Oncotarget, 2017. **8**(40): p. 66901-66911.
90. Hartmaier, R.J., et al., *Recurrent hyperactive ESR1 fusion proteins in endocrine therapy resistant breast cancer.* Ann Oncol, 2018.
91. Priedigkeit, N., et al., *Intrinsic Subtype Switching and Acquired ERBB2/HER2 Amplifications and Mutations in Breast Cancer Brain Metastases.* JAMA Oncol, 2017. **3**(5): p. 666-671.
92. Uhlen, M., et al., *Tissue-based map of the human proteome.* Science, 2015. **347**(6220).
93. Jing, S., et al., *GDNF-Induced activation of the RET protein tyrosine kinase is mediated by GDNFR-a, a novel receptor for GDNF.* Cell, 1996. **85**: p. 1113-1124.
94. Airaksinen, M.S. and M. Saarma, *The GDNF family: signalling, biological functions and therapeutic value.* Nat Rev Neurosci, 2002. **3**(5): p. 383-94.
95. Morandi, A., I. Plaza-Menacho, and C.M. Isacke, *RET in breast cancer: functional and therapeutic implications.* Trends Mol Med, 2011. **17**(3): p. 149-57.
96. Sariola, H. and M. Saarma, *Novel functions and signalling pathways for GDNF.* J Cell Sci, 2003. **116**(Pt 19): p. 3855-62.
97. Kan, Z., et al., *Diverse somatic mutation patterns and pathway alterations in human cancers.* Nature, 2010. **466**(7308): p. 869-73.
98. Roskoski, R., Jr. and A. Sadeghi-Nejad, *Role of RET protein-tyrosine kinase inhibitors in the treatment RET-driven thyroid and lung cancers.* Pharmacol Res, 2018. **128**: p. 1-17.
99. Anderson, R., D. Newgreen, and H. Young, *Neural Crest and the Development of the Enteric Nervous System.* Madame Curie Bioscience Database: Landes Bioscience, 2000-2013.
100. Plaza-Menacho, I., et al., *Targeting the receptor tyrosine kinase RET sensitizes breast cancer cells to tamoxifen treatment and reveals a role for RET in endocrine resistance.* Oncogene, 2010. **29**(33): p. 4648-57.
101. He, S., et al., *GFRalpha1 released by nerves enhances cancer cell perineural invasion through GDNF-RET signaling.* Proc Natl Acad Sci U S A, 2014. **111**(19): p. E2008-17.
102. Johannessen, C.M., et al., *COT drives resistance to RAF inhibition through MAP kinase pathway reactivation.* Nature, 2010. **468**(7326): p. 968-72.
103. Yang, X., et al., *A public genome-scale lentiviral expression library of human ORFs.* Nat Methods, 2011. **8**(8): p. 659-61.
104. Askoxylakis, V., et al., *Preclinical Efficacy of Ado-trastuzumab Emtansine in the Brain Microenvironment.* J Natl Cancer Inst, 2016. **108**(2).
105. Valiente, M., et al., *Serpins promote cancer cell survival and vascular co-option in brain metastasis.* Cell, 2014. **156**(5): p. 1002-16.
106. *3D Cell Culture*. Methods in Molecular Biology, ed. Z. Koledova. 2017: Humana Press.
107. Barretina, J., et al., *The Cancer Cell Line Encyclopedia enables predictive modelling of anticancer drug sensitivity.* Nature, 2012. **483**(7391): p. 603-7.
108. Boulay, A., et al., *The Ret receptor tyrosine kinase pathway functionally interacts with the ERalpha pathway in breast cancer.* Cancer Res, 2008. **68**(10): p. 3743-51.
109. Gattelli, A., et al., *Ret inhibition decreases growth and metastatic potential of estrogen receptor positive breast cancer cells.* EMBO Mol Med, 2013. **5**(9): p. 1335-50.
110. Hiraguri, S., et al., *Mechanisms of Inactivation of E-Cadherin in Breast Cancer Cell Lines.* Cancer Res, 1998. **58**.

111. Tasdemir, N., et al., *Comprehensive 2D and 3D phenotypic characterization of human invasive lobular carcinoma cell lines.* 2018.
112. Zhang, B.L., et al., *MiRNAs Mediate GDNF-Induced Proliferation and Migration of Glioma Cells.* Cell Physiol Biochem, 2017. **44**(5): p. 1923-1938.
113. Spanheimer, P.M., et al., *Distinct pathways regulated by RET and estrogen receptor in luminal breast cancer demonstrate the biological basis for combination therapy.* Ann Surg, 2014. **259**(4): p. 793-9.
114. Pirnia, F., et al., *Mytomycin C induces apoptosis and caspase-8 and -9 processing through caspase-3 and Fas-independent pathway.* Cell Death and Differentiation, 2002. **9**: p. 905-914.
115. Kargi, A.Y., M.P. Bustamante, and S. Gulec, *Genomic Profiling of Thyroid Nodules: Current Role for ThyroSeq Next-Generation Sequencing on Clinical Decision-Making.* Mol Imaging Radionucl Ther, 2017. **26**(Suppl 1): p. 24-35.
116. Nikiforova, M.N., et al., *Targeted next-generation sequencing panel (GlioSeq) provides comprehensive genetic profiling of central nervous system tumors.* Neuro Oncol, 2016. **18**(3): p. 379-87.